



## RESEARCH ARTICLE

# Early life trauma increases threat response of peri-weaning rats, reduction of axo-somatic synapses formed by parvalbumin cells and perineuronal net in the basolateral nucleus of amygdala

Adrienne N. Santiago<sup>1,2,3</sup>  | Kayla Y. Lim<sup>1</sup> | Maya Opendak<sup>2,3</sup> | Regina M. Sullivan<sup>2,3†</sup> | Chiye Aoki<sup>1†</sup> 

<sup>1</sup>Center for Neural Science, New York University, New York, New York

<sup>2</sup>Emotional Brain Institute, Nathan Kline Institute, New York University School of Medicine, New York, New York

<sup>3</sup>Department of Child and Adolescent Psychiatry, NYU School of Medicine, New York, New York

**Correspondence**

Chiye Aoki, PhD, Center for Neural Science, 4 Washington Place, Rm 809, New York, NY 10003.

Email: ca3@nyu.edu

**Funding information**

National Institute of Mental Health, Grant/Award Number: R21MH105846; National Institutes of Health, Grant/Award Numbers: F31 MH112372, F32MH112232, R37HD083217

**Abstract**

Early life trauma is a risk factor for life-long disorders related to emotional processing, but knowledge underlying its enduring effect is incomplete. This study was motivated by the hypothesis that early life trauma increases amygdala-dependent threat responses via reduction in inhibition by parvalbumin (PV) interneurons and perineuronal nets (PNN) supporting PV cells, thus increasing excitability of the basolateral amygdala (BLA). From postnatal day (PN) 8–12, rat pups of both sexes were reared under normal bedding or under insufficient nest-building materials to induce maternal-to-infant maltreatment trauma (Scarcity-Adversity Model, SAM). At weaning age of PN23, the SAM group exhibited increased threat responses to predator odor. The SAM-induced increase in threat response was recapitulated in normally reared PN22–23 rats that were unilaterally depleted of PNN in the BLA by the enzymes, chondroitinase-ABC plus hyaluronidase at PN19–20. Light and electron microscopic analysis of the BLA revealed that anterior-to-mid levels of SAM group's BLAs exhibited decreased PNN intensity and decreased axo-somatic synapses between PV-to-principal pyramidal-like neurons and PV-to-PV. PV and PNN densities (cells/mm<sup>2</sup>) in the BLA of both control (CON) and SAM groups were still low at PN12 and SAM delayed the ontogenetic rise of PV intensity and PNN density. Moreover, PV cell density in the anterior-to-mid BLA correlated negatively with threat response of CON animals, but not for SAM animals. Thus, reduction of PNN-supported, PV-mediated somatic inhibition of pyramidal cells provides a mechanistic support for the enduring effect of early life maltreatment manifested as increasing innate threat response at weaning.

**KEYWORDS**

amygdala, infant maltreatment, innate fear, predator odor, parvalbumin, perineuronal net, PNN, RRID: AB\_477329

**1 | INTRODUCTION**

Environment shapes postnatal neurodevelopment to produce adaptive individual differences in ecologically relevant responses (Aoki & Erisir, 2013; Hane & Fox, 2016). However, early life trauma, especially when associated with maltreatment by a caregiver, can go beyond adaptation to initiate pathology involving heightened amygdala-

dependent responses to threat, including childhood anxiety and post-traumatic stress disorder (Fareri & Tottenham, 2016; Heim & Nemeroff, 2001; Malter Cohen et al., 2013; Teicher, Samson, Anderson, & Ohashi, 2016; Tottenham, 2012). Rodent and non-human primate models of early life trauma associated with maternal maltreatment demonstrate a causal role for the amygdala in infant heightened responses to threat (Callaghan, Sullivan, Howell, & Tottenham, 2014; Drury, Sanchez, & Gonzalez, 2015; Gunnar, Hostinar, Sanchez, Tottenham, & Sullivan, 2015; Sanchez, Ladd, & Plotsky, 2001; Santiago,

<sup>†</sup>Senior authors

Aoki, & Sullivan, 2017). Here, we assess amygdala neural circuitry following an infant maltreatment paradigm previously shown to produce heightened amygdala-dependent responses to threat—the Scarcity-Adversity Model (SAM). In the SAM, the mother is provided with insufficient bedding for nest building (Roth & Sullivan, 2005; Walker et al., 2017). This manipulation results in weanlings' exhibition of enhanced fear responses to predator odor and enhanced response of the basolateral nucleus of the amygdala (BLA; Perry et al., in revision), with behavioral modifications enduring into adulthood (Perry & Sullivan, 2014).

The BLA of older pups and adults is well-recognized to be active during both learned and innate threat responses (Parkes & Westbrook, 2010; Perry, Al Ain, Raineke, Sullivan, & Wilson, 2016; Takahashi, Hubbard, Lee, Dar, & Sipes, 2007) and anxiety-like behavior (Janak & Tye, 2015; Tye et al., 2011). However, relatively less is known about the effects of this trauma on BLA synaptic circuitry and of its involvement in aberrant threat responses at weaning and pre-weaning ages. We chose to focus on parvalbumin (PV) cells, which control excitability of principle excitatory neurons that are commonly referred to as pyramidal cells (McDonald, Mascagni, Mania, & Rainnie, 2005) and produce synchronous firing in the BLA (Ryan et al., 2012). Moreover, perineuronal nets (PNNs), comprised of chondroitin sulfate proteoglycans, can encapsulate (Baker, Gray, & Richardson, 2017; Pantazopoulos, Murray, & Berretta, 2008;) and enhance excitability of some PV cells (Balmer, 2016), especially in the anterior and mid-levels of the BLA (Morikawa, Ikegaya, Narita, & Tamura, 2017). Our investigation of PNN was prompted by the finding that postnatal experience influences the ontogeny of PV/PNN in the sensory cortex (Pizzorusso et al., 2002) and that PV cells, together with PNN, in turn, modulate experience-dependent synaptic plasticity in neocortex (Pizzorusso et al., 2002). We reasoned that BLA, which exhibits cortex-like cellular composition (McDonald et al., 2005), may also exhibit experience-dependent maturation of the PV/PNN system. Moreover, PNN in the BLA protects fear memories from erasure (Gogolla, Caroni, Luthi, & Herry, 2009), indicating BLA PNN's importance in threat response. Finally, PVs and PNNs undergo dramatic increases in number and intensity within the BLA during pre-weaning ages (Berdel & Morys, 2000; Gogolla et al., 2009; Horii-Hayashi, Sasagawa, Matsunaga, & Nishi, 2015; Legaz et al., 2005), suggesting that SAM may influence this developmental trajectory.

Taken together, these findings prompted us to examine whether early life trauma from the caregiver induces heightened threat response among animals due to disturbance in pre-weaning ontogeny of PV/PNN system in the BLA, thereby contributing to the reported hyper-excitability of the BLA (Perry et al., in revision). Human neurobiology has also shown that fear conditioning is impaired after unilateral temporal lobectomy (LaBar, LeDoux, Spencer, & Phelps, 1995). This finding prompted us to examine the impact of unilateral PNN dissolution in the BLA upon innate threat response of weanlings. Our light and electron microscopic data, together with threat response analyses, provide mechanistic support linking innate fear following early life trauma to lasting weakening of *gamma*-aminobutyric acid (GABA)/PNN innervation in the anterior-to-mid BLA.

## 2 | MATERIALS AND METHODS

### 2.1 | Subjects

All procedures pertaining to the use of live rats were approved by the Institutional Animal Care and Use Committee, and followed National Institutes of Health guidelines.

Male and female Long-Evans rat pups were bred and housed with their mother in polypropylene cages (34 cm × 29 cm × 17 cm) with wood chips and ad libitum food and water, in a temperature (20 °C), humidity, and light (12 hr light/dark cycle) controlled room at Nathan Kline Institute, New York. Because pups at weaning age (~postnatal day 23, PN23) exhibit defensive response to predator odor (Perry et al., 2016; Takahashi et al., 2007; Wiedenmayer & Barr, 2001) and exhibit a significant increase in PNN density between PN21 and PN23 (Gogolla et al., 2009), we chose weaning age as a focal point for our study of PV and PNN density and intensity. Thus, we performed light and electron microscopy as well as functional assessment of this age group to investigate our primary hypothesis that SAM compromises PV and PNN integrity in the BLA. Our secondary hypothesis, that SAM alters the trajectory of PV and PNN development in the BLA, led to the ontogeny study that linked the age point of trauma (PN12) through weaning age.

### 2.2 | Scarcity-adversity model

Maternal maltreatment was experienced by half of all animals in this study, using SAM to model a low resource environment. In this model, mothers were provided with insufficient bedding for nest building (100 mL of wood shavings). This paradigm produces altered maternal care, characterized by scattering of the litter, aggressive grooming, rough transport by limbs, and trampling of pups. In spite of these maltreatments, pups gain weight normally (Raineke et al., 2015; Raineke, Cortés, Belnoue, & Sullivan, 2012; Rincón-Cortés & Sullivan, 2016). SAM complements the more severe Fragmentation Model, where removal of nesting material is combined with a grid floor and no cage cleaning, which produces more pronounced neurobehavioral effects, significant weight loss at weaning, and limbic epileptic seizures (Dube et al., 2015; Walker et al., 2017). Pups were reared undisturbed for the first week of life, except for cage cleaning. From PN8–12, 9 litters with the mother assigned to the SAM group were housed with 100 mL of bedding. Ten more litters with the mother assigned to the control (CON) group were housed with standard amount of bedding in the same animal room concurrently. All litters were video recorded during the light cycle with Ethovision software (Noldus, Leesburg, VA) and behavioral observations were recorded over two to three 30 min periods using Clicker software to validate maternal treatment of pups (Figure 1).

### 2.3 | Predator odor test

P23 (weaning age) pups exhibit defensive response to predator odor, including novel male odor and fox urine (Perry et al., 2016; Takahashi et al., 2007; Wiedenmayer & Barr, 2001). To assess whether SAM altered weaning-age defensive responses compared to control rearing, SAM and CON rats were subjected to a predator odor test. Pups'

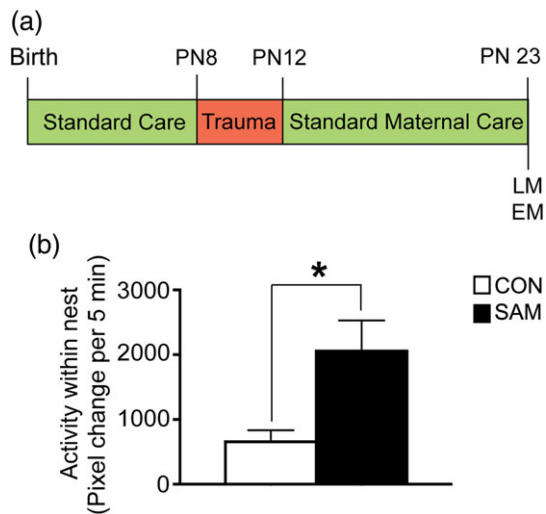


**FIGURE 1** Scarcity model of early life trauma. Panel (a): Schematic of the SAM of low resources. Mothers are deprived of bedding for 5 days between PN8 and PN12. At PN23, brains of rats were perfused for the light microscopy experiments (LM) and EM experiments. Panel (b): SAM induces maternal maltreatment characterized by an increase in mothers stepping on, throwing, and dragging pups (see Table 1). Together, these values correspond to within-nest activity, which is significantly increased for the SAM litters ( $N = 4$  SAM litters,  $N = 4$  CON litters). “Within-nest activity” was measured as pixel change per 5 min, digitized using Ethovision [Color figure can be viewed at [wileyonlinelibrary.com](http://wileyonlinelibrary.com)]

responses to predator odor were explored with two tests: approach-avoidance in open field and a Y-maze test.

**Open field:** Pups were acclimated for 5 min to a 24 × 24-in Plexiglas arena, then exposed for 5 min to 1 mL of fox urine on a Kimwipe, placed in the corner of the arena. Proximity to the predator odor was assessed with Ethovision software (“mean distance to zone,” in cm, calculated as the mean distance averaged over each frame and binned by minute). Animals were euthanized 2.5 hr later by transcardial perfusion with aldehydes, as described below under “Brain tissue preparation,” to assess PV immunoreactivity and PNN labeling within the BLA of these brains.

Y-maze consisted of a start box (7 cm long and 9 cm wide) and two alleys (22 cm long and 9 cm wide) extending at 45° angles. The start box was separated from the alleys via two removable doors. One arm of the maze contained the familiar odor of clean bedding (20 mL of clean, aspen shavings), while the other arm contained the odor of a novel adult male

delivered through an olfactometer at a flow rate of 3 L/min, 1:10 odor: air. For each trial, the pup was given 1 min to make a choice. It was considered a choice when the pup's entire body entered the alleyway of an arm. Each pup was placed in the start box for 5 s for habituation before the doors to the alleys were removed. Each subject was given five sequential trials, and the floor was cleaned between each trial. Pup orientation was counterbalanced between trials. Observations of each pup were made blind to the rearing condition.

## 2.4 | Histological procedures for the weaning age animals and for the ontogeny study

Sixteen subjects of both sexes were perfused at each of the four age groups: PN23–24, PN18–19, PN15–16, and PN11–12. These age groups will be referred to as “PN23,” “PN18,” “PN15,” and “PN12” for short. Of the 16 subjects of each age group, 7 or 8 pups (7 pups of PN18 and 8 pups of the other age groups), derived from 10 litters (no more than 1 male and 1 female per litter) were reared with standard bedding. The remaining 8 or 9 pups of the age group (9 pups for PN18 and 8 pups for the other age groups), derived from 9 litters (no more than 1 male and 1 female per litter), were reared with limited bedding, as described above under “Scarcity-Adversity Model.” Brains from these animals were used to characterize developmental changes of PV cells and PNN within the BLA. Just prior to perfusion, PN23 animals were subjected to a fox urine predator odor test, as is described above.

### 2.4.1 | Brain tissue preparation

Following predator odor response testing, rat pups were given an IP injection of urethane (1.5 g/kg) to induce a state of deep anesthesia under which the subject was unresponsive to a strong foot pinch. Subjects were then transcardially perfused with 50 mL of 0.01 M phosphate buffered saline (pH 7.4; PBS) with heparin (4,000 U/L) followed by 500 mL of 4% paraformaldehyde in 0.1 M phosphate buffer (pH 7.4) at a flow rate of 50 mL/min. Brains were post-fixed in phosphate buffered 4% paraformaldehyde at room temperature for 3 days and at 4 °C for at least 2 weeks. Tissue was secured in agar and sectioned using a vibrating microtome (VT1000 S, Leica Microsystems, Wetzlar, Germany) at a thickness set to 55 μm. All amygdala-containing sections (Bregma –1.88 to –3.80 mm) were collected, and analyzed histologically at 550 μm intervals along the antero-posterior

**TABLE 1** Frequency of mother-pup interaction behaviors of SAM and CON litters during PN8–12

| Percent of observations in which behaviors occurred. |                         |                     |                 |          |
|--|-------------------------|---------------------|-----------------|----------|
|  | Low bedding (%) $N = 6$ | Control (%) $N = 5$ | <i>t</i> test   | <i>p</i> |
| <b>Atypical behaviors</b>                            |                         |                     |                 |          |
| Rough handling                                       | 17.13 ± 8.07            | 0.00 ± 0.00*        | $t(9) = 2.734$  | 0.0231   |
| Stepping on pups                                     | 21.76 ± 7.45            | 0.00 ± 0.00*        | $t(9) = 2.918$  | 0.0171   |
| Pup vocalizations                                    | 13.33 ± 9.72            | 2.22 ± 1.62         | $t(9) = 1.309$  | 0.2231   |
| Scattered nest                                       | 16.67 ± 4.36            | 3.33 ± 3.33*        | $t(9) = 2.345$  | 0.0436   |
| <b>Typical behaviors</b>                             |                         |                     |                 |          |
| Mother in nest                                       | 67.22 ± 9.15            | 75.93 ± 5.9         | $t(9) = 0.8273$ | 0.4295   |
| Nursing  | 53.24 ± 8.49            | 72.22 ± 4.65        | $t(9) = 1.845$  | 0.0982   |

The percentages in the table were calculated as described previously (Rainecki, Moriceau, & Sullivan, 2010). The table shows the proportion of observation periods that showed the itemized behavior per litter, averaged across several litters.

axis (AP) of the amygdala. To prevent bacterial growth, sections were stored at 4 °C in 0.01 M PBS containing 0.05% sodium azide.

#### 2.4.2 | Antibody characterization

PV was identified by immunohistochemical labeling using a monoclonal mouse anti-PV antibody (Sigma-Aldrich, St Louis, MO, Cat# P3088, RRID: AB\_477329) at a dilution of 1:10,000. Western blot analysis of whole brain homogenate yields a single band at ~12 kDa (data provided by Sigma-Aldrich and confirmed by [Celio & Heizmann, 1981]), the molecular weight of PV protein. Specificity has been determined by preadsorption controls, which eliminate labeling in Western blot and histology (Celio & Heizmann, 1981; Hackney, Mahendrasingam, Penn, & Fettiplace, 2005). This antibody has been used previously for both light and electron microscopic studies (Fitzgerald, Chan, Mackie, Lupica, & Pickel, 2012; Rainnie, Mania, Mascagni, & McDonald, 2006), and electrophysiological studies confirm that the antibody exclusively labels fast-spiking cells (Zaitsev et al., 2005).

#### 2.4.3 | PV labeling

Staining of the sections from the ontogeny set, ranging from PN12 to PN23 was conducted on a single day, in parallel, so as to maintain homogeneity of all reagents. To enhance the antibody's permeation of tissue, free-floating vibratome sections underwent a freeze/thaw protocol, for which tissue was cryoprotected in increasing concentrations of dimethyl sulfoxide (DMSO; 5%, 10%, and 20%) for 10 min each before rapid freezing in a beaker of 2-methylbutane chilled to -78.5 °C using dry ice and 100% ethanol as the heat conduit. After rapid freezing, the tissue was thawed by immersing in a bath of 20% DMSO at room temperature, before another bout of rapid freezing for a total of 8 freeze/thaw sequences. Tissue was then incubated in decreasing concentrations of DMSO (10% and 5%) for 5 min each before returning to PBS. Tissue was then treated with 1% hydrogen peroxide in 0.01 M PBS for 30 min, washed with 0.01 M PBS, and blocked in 0.01 M PBS containing 0.05% sodium azide and 1% bovine serum albumin (PBS-BSA-Azide) for 1 hr. After ~48-hr incubation at room temperature with the mouse anti-PV antibody diluted in PBS-BSA-Azide (1:10,000), tissue was washed with PBS and incubated for 1 hr in biotinylated goat-anti-mouse IgG secondary antibody (Vector laboratories, Burlingame, CA, cat# BA-9200, dilution 1:200). Tissue was then washed in 0.01 M PBS, incubated in a solution of the Vectastain Elite ABC HRP kit (Vector Laboratories, Burlingame, CA, cat# PK-6100), washed with 0.01 M PBS, and incubated for 9 min in a filtered solution of 3',3'-diaminobenzidine tetrahydrochloride (DAB; 10 mg tablet, Sigma Aldrich in 44 mL of PBS buffer), catalyzed by 0.003% hydrogen peroxide. The peroxidase reaction was terminated by washing the tissue in 0.01 M PBS to remove the substrate. Tissue was washed further, then mounted on gelatin and chromium potassium sulfate dodecahydrate-coated slides and coverslipped using Permount (Fisher Scientific, Hampton, NH, cat# SP15), and later imaged on the Olympus VS120 at magnifications of 2× and 10×.

#### 2.4.4 | PNN labeling

Chondroitin sulfate proteoglycans of PNNs were identified in a separate set of vibratome sections by tagging the biotinylated form of

the lectin, *Wisteria floribunda* agglutinin (WFA; Sigma-Aldrich cat# L1516; dilution 1:200) that bound to proteoglycans. Staining of the sections from the ontogeny set was conducted in parallel, so as to maintain homogeneity of all reagents. Similarly, staining of the sections of brains from the animals that underwent PNN-dissolution, then the Y-maze test were performed in parallel, so as to minimize inter-animal differences resulting from differences in the reagents. Tissue was treated with 1% hydrogen peroxide in 0.01 M PBS for 30 min, washed with 0.01 M PBS, and blocked in 0.01 M PBS containing 0.05% sodium azide, 0.5% Triton X-100, and 1% bovine serum albumin (PBS-BSA-Triton-Azide) for 1 hr. After a two-night incubation in PBS-BSA-Triton-Azide containing biotinylated WFA, tissue was treated with Vectastain Elite ABC, visualized with DAB (0.02%) and 0.003% hydrogen peroxide, mounted on gelatin and chromium potassium sulfate dodecahydrate-coated slides and imaged as described above.

#### 2.4.5 | PNN labeling specificity test

Specificity of proteoglycan staining with WFA was verified by intracranial injection at PN23 of the PNN-dissolving enzymes. Rats were anesthetized with isoflurane (Fisher scientific) at PN23 and infused with the PNN-dissolving enzymes, chondroitinase ABC (Sigma-Aldrich, CAT# C3667, Enzyme Commission Number EC 4.2.2.4) and hyaluronidase (Sigma-Aldrich, CAT# H4272, Enzyme Commission number EC 3.2.1.35), while anesthetized with isoflurane (Fisher Scientific) and with the head secured using a stereotaxic instrument (Kopf, Tujunga, CA). Anesthesia was maintained with a flow of isoflurane (1%) in oxygen. A total of 0.3 µL of sterile saline containing 0.01 U chondroitinase ABC and 0.7 mg of hyaluronidase was delivered at a rate of 0.1 µL/min via a Harvard syringe pump, which used PE10 tubing to connect two 0.5 mL Hamilton syringes to bilateral cannula inserts (PlasticsOne) placed into the BLA. The stereotaxic coordinates used were AP -1.6 mm from Bregma, ML ±4.8 mm and DV -6.9 mm from cortical surface. After surgery, animals were sutured and returned to the nest for recovery, then euthanized by transcardial perfusion on the following day for labeling brain tissue for PNN in the BLA as was as described above. Several labs have documented that chondroitinase ABC with hyaluronidase selectively dissolves proteoglycans without destroying BLA tissue (Balmer, 2016; Gogolla et al., 2009). Intactness of neuronal density of the BLA and adjacent brain structures was verified by Nissl staining.

#### 2.4.6 | Light microscopic dual labeling for PV and PNN

In order to determine the proportion of PNNs surrounding PV versus non-PV cells, dual labeling of single sections was performed. Sections were freeze-thaw treated and stained for PNN with WFA lectin, as described above, under "PNN labeling." Following the last post-DAB washes, tissue were blocked in PBS/BSA/azide for 1 hr and incubated in PV primary antibody, as described above, under "PV labeling." After overnight incubation, tissue were washed with 0.01 M PBS and incubated for 1 hr in biotinylated goat-anti-mouse IgG secondary antibody. Tissue was then washed in 0.01 M PBS, incubated in a solution of the Vectastain Elite ABC HRP kit, washed with 0.01 M PBS, and incubated for 9 min in a filtered solution of DAB plus 0.05% cobalt

chloride (Sigma, cat# C-2644) catalyzed by 0.003% hydrogen peroxide, for a black reaction product. The peroxidase reaction was terminated by washing the tissue in 0.01 M PBS to remove the substrate. Tissue was washed further, then mounted on gelatin and chromium potassium sulfate dodecahydrate-coated slides and coverslipped using Permount (Fisher Scientific, cat# SP15), and later imaged on the Olympus VS120 at magnifications of 2 $\times$  and 10 $\times$ .

#### 2.4.7 | Light microscopic quantification of PV and PNN

BLA contours were defined according to Paxinos and Watson's brain atlas (Paxinos & Watson, 1998), which outlines the basolateral subnuclei of amygdala (BLA). This is in contrast to common references to the "basolateral complex," which includes the lateral subnucleus, which we excluded from our BLA contours.

All PV and PNN quantifications were performed by persons blind to the experimental condition. ImageJ (NIH) was used for quantification of the density (number of cells per unit area) and intensity of somata immunoreactive for PV and WFA (i.e., PNN-labeled). Intensity was measured as the grayscale value on a scale of 0 (white) to 255 (black).

Intensity of PV+ cells was sampled at the cytoplasm. To provide a control for possible between-brain variation in intensity labeling, a background measure was sampled by measuring the grayscale of nuclei, which remained unlabeled. This value was subtracted from the grayscale measure of each PV cell's perikaryal cytoplasm for the final PV cytoplasm intensity. The value of 25 was set as the threshold for considering a cell body to be PV+. Success of immunocytochemical detection of PV was confirmed through verification of immunopositive perikarya in the hippocampus and reticular thalamic nuclei. Using this measure, brains of all subjects were considered successfully immunolabeled, even when no positive staining was visible in the amygdala.

PNN labeling was defined as darker WFA labeling around a cell body, with some cells exhibiting WFA labeling along proximal dendrites. Loosely arranged proteoglycans are present in the extracellular matrix (ECM) without clustering around any particular nucleus to form PNN, and the grayscale intensity value of this more diffuse labeling was measured by taking a  $\sim 50 \mu\text{m}^2$  sample of tissue containing no PNN. The grayscale intensity value of PNN labeling was measured in three different ways: (1) the grayscale value of the PNN was sampled; (2) in the subset of PN23 brains, a grayscale value for unlabeled soma was obtained and subtracted from the PNN intensity measure to assess possible between-brain variation in intensity labeling; (3) for the tissue of animals that were tested on the Y-maze predator odor test two days after enzymatic dissolution of PNN, intensity of WFA labeling representing the intensity of PNN and the loosely arranged proteoglycans was measured for the BLA and normalized to the WFA labeling of the immediately adjacent perirhinal cortex (posterior agranular insular cortex).

For each animal of the ontogeny study set, the average density and intensity values of PV and PNNs were determined separately for the anterior-to-mid (Bregma  $-2.56$  to  $-2.8$  mm) versus the more posterior levels of the BLA. For animals that underwent Y-maze test

following enzymatic dissolution of PNN, intensity of WFA labeling was measured at the anterior-to-mid level only.

For all PV and PNN analyses, each animal was considered an independent entity (i.e.,  $N = \text{animal}$ ) that could respond to environmental and developmental factors. Two-way ANOVAs were conducted to assess the main effect of the rearing condition or of the ages, followed by Fisher's post hoc analysis to assess rearing effects within each age-group or age-effect within each rearing group.

#### 2.5 | PNN dissolution-threat response test

To assess the potential role of PNN in the BLA-dependent threat response, defensive responses to predator odor following dissolution of PNN was assessed, using a Y-maze odor choice test. A cohort of 24 rats aged PN19–20 underwent a surgical procedure for determining the impact of BLA PNN dissolution upon threat response. These rats were divided into three groups (4 males and 4 females per group): CON-S (control-reared, with saline injected), CON-E (control reared, with the PNN-dissolving enzyme injected), and SAM-S (SAM-reared and saline injected). The procedure for infusion of the PNN-dissolution was exactly as described above for testing specificity of the PNN labeling. Two days after this procedure, at age PN21/22, pups were tested on the Y-maze. Because ChABC-hyaluronidase injection impedes PV-mediated inhibition (Balmer, 2016), subjects were monitored for seizure for 5–6 days following injection, in contrast to the "PNN labeling specificity test," which was performed 1 day following injection. Animals were euthanized by transcardial perfusion with aldehydes, as described above, "Brain tissue preparation," at ages ranging from PN24 to PN26. PNN dissolution by the enzymes was verified by the PNN labeling procedure described above, except that the values were quantified for intensity of biotinylated WFA labeling of the entire BLA, including the ECM beyond the PNN, normalized to the labeling intensity in the perirhinal cortex immediately adjacent to the BLA, so as to assess PNN dissolution that was specific to the BLA. To verify intactness of the BLA that received ChABC-hyaluronidase injection, PNN-labeled sections were stained with Nissl.

#### 2.6 | Electron microscopy

##### 2.6.1 | EM tissue processing

Vibratome sections from the weaning-aged (PN23) and ontogeny study at  $\sim$ Bregma  $-2.56$  to  $-2.8$  mm were taken for further analysis using the electron microscope (EM). These sections were immunostained for PV as described above, and then processed for EM (Aoki, Rodrigues, & Kurose, 2000; Farb, Aoki, & Ledoux, 1995; Wable et al., 2014). Specifically, after terminating the HRP-DAB reaction, tissue was washed with 0.01 M PBS and then post-fixed with 2% glutaraldehyde for 16 min at room temperature. Tissue was then washed in 0.01 M PBS, washed again in 0.1 M PB, transferred to ceramic multiwell dishes (Coors) and incubated for 1 hr in 1% osmium tetroxide ( $\text{OsO}_4$ ). After rinsing with 0.1 M PB, tissue was rapidly dehydrated in increasing concentrations of ethanol (30%, 50%, and 70%) before overnight incubation in 70% ethanol containing 1% uranyl acetate (UA) at 4  $^\circ\text{C}$  while photoprotected by foil. Tissue was then rinsed in



70% ethanol and further dehydrated in 90% and 100% ethanol (2 $\times$ ), acetone ACS grade, Electron Microscopy Sciences (EMS; 3 $\times$ ), before immersion in 1:1 acetone: EPON (EMbed 812 embedding resin, DDSA, NMA, DMP30, EMS) for 1 hr at 50 °C and 3 hr at room temperature. After overnight incubation in 100% EPON, tissue was flat-embedded between Aclar sheets, weighted, and cured at 60 °C for ~36 hr. BLA from flat-embedded tissue was then capsule-embedded and sectioned into 70 nm ultrathin sections with an ultramicrotome (MT-7, RMC Boeckeler, Tucson, AZ). Sections were mounted on nickel grids (EMS cat# 15800) that had been coated in 0.3% Formvar (EMS) in ethylene dichloride under low-humidity conditions, and then counterstained with Reynold's lead citrate.

## 2.6.2 | EM quantification

All EM image acquisitions and quantifications were performed by persons blind to experimental condition. From each of six SAM and six CON brains at age P23, cell bodies of 10 PV-immunoreactive inhibitory interneurons and 10 pyramidal neurons were sampled from the anterior-to-mid level of the BLA. Thus, from each animal, a total of 20 cell bodies were sampled. Cell bodies were imaged at 20,000 $\times$  using the JEOL JEM1200-EX-II electron microscope and captured with the XR80 CCD camera and AMT software (Woburn, MA). To limit cell selection to the BLA subnucleus, distinguishing features of each BLA were mapped at 4 $\times$  using an Olympus camera lucida. Images of different ultrathin sections were aligned after image acquisition to ensure that the same cell was never re-analyzed from another grid. To ensure full DAB immunoreactivity of PV cells and terminals, cell profiles were only image-captured close to the EPON-tissue interface carved by the vibratome blade, where immunolabeling could be expected to be optimal. DAB labeling was only considered positive if the soma or terminal was darker than the relatively electron-dense mitochondria in the imaged region.

Cell bodies in the BLA were categorized as one of three types. Pyramidal cells were identified as distinct from interneurons by their characteristically smooth nuclear envelope, lack of asymmetric axo-somatic synapses with thick post-synaptic densities (PSDs), and lack of PV-immunoreactivity. PV cells were identified by the presence of intense immunoreactivity of the perikaryal cytoplasm to the PV-antibody. The non-PV inhibitory interneurons were identified as such, based on the lack of PV-immunoreactivity, the presence of deep indentations along the nuclear envelope, and presence of asymmetric axo-somatic synapses. Cell bodies of non-PV inhibitory interneurons were excluded from analysis for the current study.

Axon terminals forming axo-somatic synapses in the BLA were also categorized as one of three types: PV-immunoreactive and symmetric, PV-immunonegative and symmetric, and PV-immunonegative and asymmetric, the last of which were considered to belong to excitatory neurons.

For each cell body profile, three measurements were made. The lengths of axon terminals' plasma membrane forming direct contact with the cell body, i.e., free of astrocytic process intervention and less than 50 nm in distance between the axonal and cell body plasma membranes were measured. We also measured lengths of the plasma membrane of the cell body. Both of these length

measurements were made using digitally captured images using the Image J software (NIH, version 1.51). These values were used to obtain the average value of axon terminal lengths for that cell and the percent of plasma membrane of that cell body contacted by axo-somatic synapses of each type. The third measurement made for each cell body was the number of axon terminals forming axo-somatic synapses, per  $\mu\text{m}$  of cell body plasma membrane. Each neuron was considered an independent unit that could respond to alterations in levels of afferent activity from a variety of neurons within and outside of the BLA (i.e.,  $N = \text{cell}$ ). Thus, for statistical analyses, the average value of these measurements was assessed for each cell, and these "per cell" values were pooled across six SAM brains. Similarly, neurons of each type of cell were pooled from six brains of the control group (CON).

## 2.7 | Statistical analyses

First, normality of the data was determined by the Kolmogorov-Smirnov test (KS). For data that were non-Gaussian in distribution, the Mann-Whitney  $U$  test was used to compare between two groups. For data that passed the KS test, Student's  $t$  test was used to compare between two groups. For the analysis of PN23 tissue, consisting of cell density, PV and PNN intensity, and EM data, two-way ANOVA for sex versus treatment revealed no main effect for sex. Thus, data for male and female subjects were combined per treatment group. Correlations between PV density and innate response to fox urine were analyzed by linear regression, and Pearson coefficients are reported. Two-way ANOVA was used to test for interaction between rearing condition and age for the ontogeny data, followed by Fisher's post hoc analysis. For electron microscopic data, which comprised of a single age group, Student's  $t$  test was performed to test for the effect of rearing by comparing values of SAM versus CON. For all tests, error is reported as *SEM* and significance was established as  $p < .05$ . The software Prism (GraphPad Software, version 7, San Diego, CA) was used for these tests and for graph plotting.

## 3 | RESULTS

### 3.1 | Maternal observations during infant treatment

As illustrated in Figure 1 and Table 1, mother-pup interactions during the SAM rearing from PN8-12 exhibited more rough handling of pups and were more active in the nest, compared to control nests (CON;  $p = .025$ ; Figure 1b). These activities included eating, drinking, and grooming in the nest, as well as scattering and maltreatment of pups (stepping on, dragging, or throwing pups). Also notable was the lack of difference between the groups with regard to nursing or mother's proportion of time in the nest. This fits with the absence of effect of SAM upon pups' body weight gains. All of these findings replicate the behavioral patterns published previously by the Sullivan lab (Perry & Sullivan, 2014; Raineki et al., 2012; Rincón-Cortés & Sullivan, 2016).

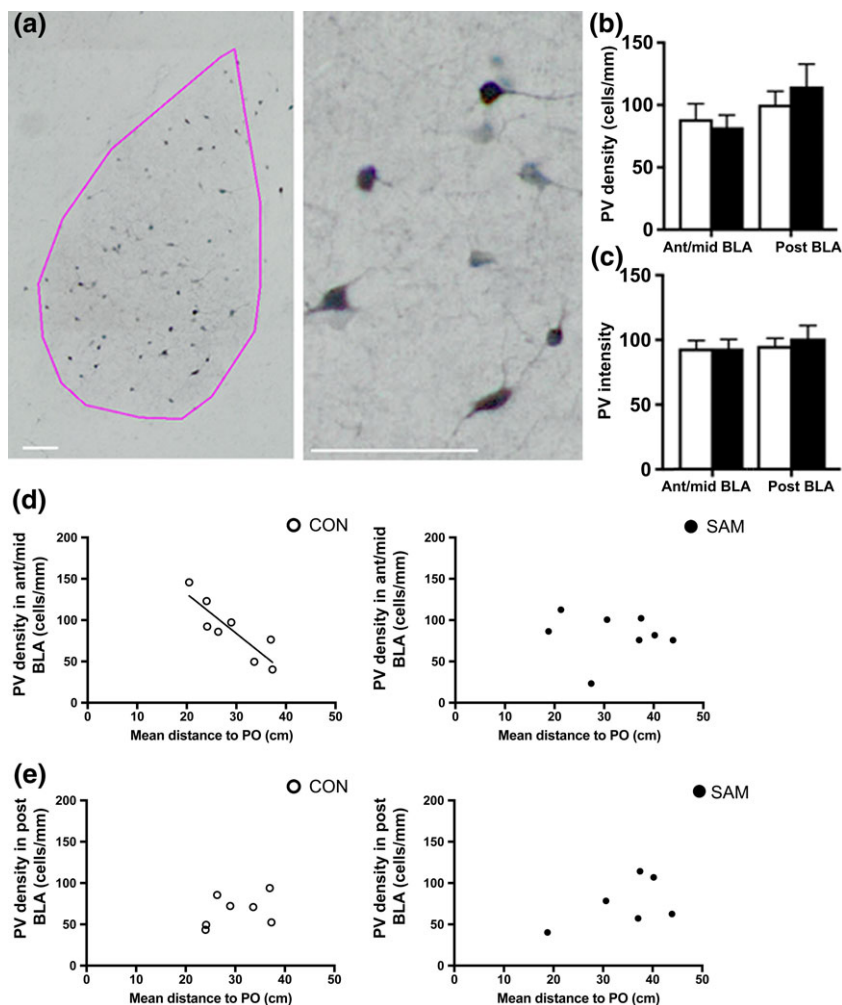


**FIGURE 2** PV cell labeling of anterior-to-mid BLA correlates with threat response to fox urine odor of CON animals but not SAM animals. (Panel a) PV cells are prominent within the BLA (pink contour) and exhibit multipolar dendrites (scale bars = 100  $\mu$ m). (Panel b) The mean values of PV density of the two rearing groups did not differ in the anterior-to-mid or posterior BLA. (Panel c): The mean values of PNN intensity also do not differ across the rearing groups, whether in the anterior-to-mid or posterior BLA. For both groups, large variance in PV density and threat response to fox urine odor was noted, measured as the mean distance, in cm, of the animal to the source of fox urine odor within a 24"  $\times$  24" area. For CON animals, this distance measurement correlated strongly and inversely with PV density in the anterior-to-mid levels of BLA ( $R = -0.868$ ,  $p = .0052$ ) (panel d). No such correlation was found for the posterior level of CON BLA ( $R = 0.40$ ,  $p = .40$ ) (panel e). PV density of SAM brains did not correlate at any level with threat response ( $R = -0.50$ ,  $p = .21$  for ant/mid-level, panel d, right;  $R = -0.08$ ,  $p = .85$  for posterior level, panel e, right) [Color figure can be viewed at [wileyonlinelibrary.com](http://wileyonlinelibrary.com)]

### 3.2 | PV cell labeling in the BLA at weaning

This anatomical study was motivated by the hypothesis that early life trauma increases amygdala-dependent threat responses due to reduction in inhibition by PV interneurons resulting in increased excitability of the BLA. Having verified that SAM group of animals experienced more rough handling by mothers, we next sought to assess the putative impact this experience from PN8–12 could have on developmental patterns of the BLA during the subsequent pre-weaning ages.

### 3.3 | PV regulation of threat response is lost following SAM

Having verified that SAM increased infant maltreatment, we next sought to determine whether this altered PV cell prevalence in the BLA of SAM animals and/or of their innate threat response, relative to CON animals', at weaning. PV cells in the BLA were multi-polar, aspiny

and evenly distributed over the BLA (Figure 2a). Quantitative analysis revealed that the group average of PV density (Figure 2b) and intensity of individual PV cells' immunolabeling in the anterior-to-mid and posterior BLA were indistinguishable ( $p = .700$  for PV density in the anterior-to-mid BLA;  $p = .5221$  for PV density in the posterior BLA;  $p = .996$  for PV intensity in the anterior-to-mid BLA;  $p = .6157$  for PV intensity in the posterior BLA).

The innate threat response of weanlings was measured as the mean distance that animals were positioned from the source of predator odor, i.e., fox urine, within a 2 ft  $\times$  2 ft arena (mean distance between the animal and the predator odor per frame, averaged per minute bin). This measurement revealed a twofold difference in individual differences for CON animals, ranging from 20 to 38 cm from predator odor. Seeing that both the animals' distance from the predator odor and PV density varied widely among animals, we asked whether these two values were correlated. Indeed, Pearson

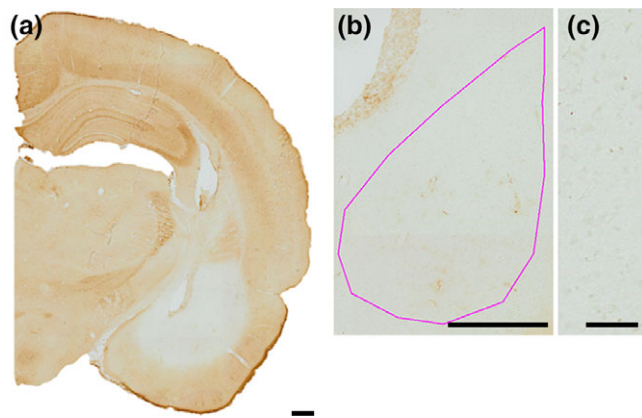


**FIGURE 3** Specificity of WFA labeling of PNN in the BLA of weanling rats. (Panel a) HRP-DAB was used to detect WFA labeling. Specificity of WFA labeling was confirmed by reduction of WFA labeling within the brains injected with the enzymes, chondroitinase-ABC and hyaluronidase, known to dissolve proteoglycans of the PNN and surrounding neuropil. The region infused with chondroitinase-ABC and hyaluronidase exhibited complete absence of the HRP-DAB reaction product, while PNN labeling remained intensely labeled in the surrounding regions (e.g., dorsal hippocampus and reticular thalamus) (scale bar = 200  $\mu\text{m}$ ). (Panel b) The pink contour indicates the boundary of the BLA (scale bar = 200  $\mu\text{m}$ ). (Panel c) The lower right panel shows detail of the enzyme-infused region (scale bar = 50  $\mu\text{m}$ ). All panels were taken at a magnification of 10 $\times$  [Color figure can be viewed at [wileyonlinelibrary.com](http://wileyonlinelibrary.com)]

correlation analysis revealed a robust correlation for CON rats ( $N = 8$ ), specifically at the ant-to-mid level of the BLA ( $p = .0052$ ;  $R = -.868$ , Figure 2d, left panel) and not for the posterior BLA ( $p = .37$ ,  $R = .40$ , Figure 2e, left panel). This negative correlation indicates that CON animals with higher densities of PV cells in the anterior-to-mid level of BLA elicited less threat response. Assuming BLA excitability is related to threat response, the increased density of PV cells could be a reflection of the increased efficacy by the PV cells to suppress BLA excitability and with it, threat response.

SAM group also exhibited large individual differences in this innate threat response at PN23, with distances to the predator odor varying from 19 to 45 cm and no significant difference in the group mean value, compared to CON's (mean<sub>CON</sub>  $\pm$  SEM = 28.98  $\pm$  2.24 cm; mean<sub>SAM</sub>  $\pm$  SEM = 32.09  $\pm$  3.21,  $p = .4406$  and  $t(14) = 0.7938$  by two-tailed unpaired  $t$  test). However, unlike the CON group, analysis of tissue from the SAM group ( $N = 8$ ) revealed no correlation between threat responsivity to the predator odor and PV density in the anterior-to-mid level of BLA ( $p = .84$ ,  $R = -.08$  Figure 2d, right panel) or in the posterior BLA ( $p = .30$ ,  $R = .51$  (Figure 2e, right panel).

### 3.4 | Assessment of WFA specificity

In the anterior-to-mid level BLA, and to a lesser extent also the posterior BLA, a subpopulation of PV neurons are encapsulated by PNN. Conversely, for the adult male mouse BLA, it has been reported that PNN encapsulates excitatory neurons in the posterior BLA, with minimal number of excitatory neurons in the anterior BLA being encapsulated by PNN. While the impact of PNN upon excitatory neurons remains unknown, PNN is known to enhance PV cells' excitability

(Balmer, 2016) which, in turn, would enhance feedback inhibition of pyramidal neurons and of pyramidal neurons' synchronous firing in the BLA (Ryan et al., 2012). Although PV density and PV intensity showed no group difference between SAM and CON, a possibility remained that PNN level undergoes changes due to SAM and that such changes contribute to innate threat response.

First, specificity of WFA labeling was confirmed by injecting BLA of PN22 CON rats with chondroitinase ABC + hyaluronidase enzymes to dissolve proteoglycans of the PNN as well as the tissue surrounding PNNs (Figure 3a). The grayscale value for BLA with dissolved proteoglycan, measured at a point central to the cannula tip on PN23 was 29.3 arbitrary units of intensity (AU) lighter than the average BLA of age-matched CON BLA without enzyme infusion and 11.8 AU darker than the average grayscale value of a slide containing no tissue. The enzymatic treatment also rendered the density of PNNs to be 0 per  $\text{mm}^2$  within the BLA (Figure 3a). The intensity resulting from enzymatic dissolution of PNN was defined to be background labeling and was <16% of the average BLA intensity value (at PN23) and < 9% of the average PNN intensity value at PN23. PN23 tissue showed distinct PNN labeling within the BLA of both CON and SAM brains at anterior-to-mid and posterior levels (Figure 4a).

Dual labeling was then performed, to estimate the proportion of PNNs surrounding PV cells. Within CON BLA of males and females at PN23, the great majority of PNNs surrounded neuronal cell bodies immunopositive for PV ( $84\% \pm 11\%$ ,  $n = 4$  animals, sampling 173 PNNs from 19 sections, spanning the anterior-to-posterior BLA from 2 female and 2 male PN23 CON brains; Figure 4b). The percentage of PNNs surrounding PV+ cells was not significantly different for the anterior-to-mid level ( $90\% \pm 8\%$ ) versus posterior level ( $80 \pm 16\%$ ) BLA by two-tailed unpaired  $t$  test ( $p = .603$ ;  $t(6) = 0.550$ ). PNNs surrounded the greater majority of neuronal cell bodies immunopositive for PV in PN23 SAM BLA as well, with no significant difference between anterior-to-mid level ( $99\% \pm 0.4\%$ ) and posterior level ( $99\% \pm 0.6\%$ ) percentage of PNN surrounding PV cells ( $p > .999$ ;  $t(6) < 0.001$ ). Over all anterior-to-posterior levels, there was no significant difference in percentage of PNN surrounding PV cells when comparing CON ( $84.17\% \pm 11\%$ ) and SAM ( $99\% \pm 0.5\%$ ;  $p = .238$ ;  $t(6) = 1.312$ ). An  $F$  test to compare variances revealed a significantly higher variance among CON versus SAM ( $p < .001$ ;  $F(3,3) = 583$ ). Together, this indicates that any detectable differences in PNN, especially in the SAM group, are likely to affect the PV population specifically, and not the population of PNN surrounded Pyr cells identified by Morikawa et al. (2017), which are likely to emerge later in development (Baker et al., 2017).

Having verified that WFA labeling reflects enzyme-sensitive PNN labeling and that the great majority of them surround PV cells, comparison of PNN labeling in BLA was made between tissue of PN23 CON animals and PN23 SAM animals. This comparison revealed a significant decrease of PNN intensity within anterior-to-mid level BLA of PN23 SAM animals, relative to the corresponding region of PN23 CON animals ( $p = .0114$  by two-tailed  $t$  test,  $t(10) = 3.093$ ) but only marginally different at the posterior level ( $p = .1208$ ,  $t(7) = 1.766$ ) (Figure 4c, lower). In contrast, there was no significant change in PNN density across the two groups for any level of the BLA ( $p = .5660$ ,  $t$



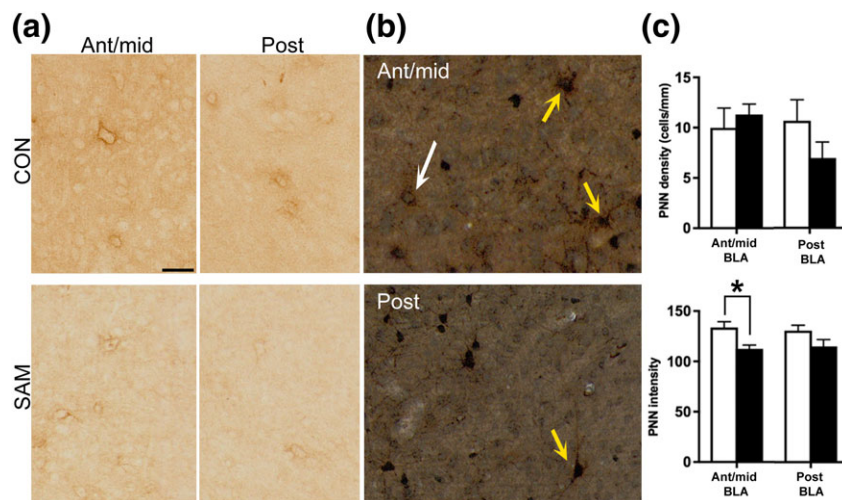


**FIGURE 4** PNN labeling at PN23. (Panel a) The putative effect of SAM upon PNN labeling in the BLA was examined at PN23. In both the anterior-to-mid and posterior levels of BLA, CON and SAM groups exhibited PNN surrounding cell bodies (scale bar = 50  $\mu$ m). (Panel b) Dual labeling for PNN by DAB (brown) and PV by silver-intensified gold immunolabeling (black) revealed PNN surrounding PV immunoreactivity, based on the blackened cell body and nuclei of the latter (yellow arrows in the anterior-to-mid and posterior BLA of CON PN23 brains). A few in the same field of view lacked the black label, indicating PNN in the absence of PV (white arrow). Images analyzed from such dually labeled tissue indicated that approximately 88% of the PNN occur surrounding PV cells (scale bar = 50  $\mu$ m). (Panel c) PNN density (upper panel) and intensity of PNNs (lower panel) were compared between SAM and CON groups. The comparisons revealed significant difference for PNN intensity in the anterior-to-mid level, indicated by asterisks ( $p < .05$ ) [Color figure can be viewed at [wileyonlinelibrary.com](http://wileyonlinelibrary.com)]

(10) = 0.5935 for anterior-to-mid BLA;  $p = .1923$ ,  $t(7) = 1.443$  for posterior BLA; Figure 4c, upper).

### 3.5 | PNN dissolution of CON animals enhances innate threat response, as it does for SAM animals

In order to assess whether this change in PNN intensity within SAM BLA in the anterior-to-posterior levels could contribute to the enhanced innate threat response of SAM animals, we tested the impact of experimentally reducing PNNs in the BLA of CON animals. Innate threat responding to a predator odor, novel adult male, was assessed using a Y-maze odor choice test. Weanlings of the CON group that were given the PNN-dissolving enzyme targeted at the BLA (CON-E) made fewer choices toward male odor ( $1.750 \pm 0.31$ ), relative to the choices made by age-matched CON weanlings that also received intra-amygdala saline infusion (CON-S;  $2.625 \pm 0.31$ ) ( $p = .0356$  by one-way ANOVA;  $p = .011$ ,  $t(21) = 2.792$ , comparing CON-E versus CON-S by Fisher's post hoc analysis, Figure 5a). The elevated avoidance of predator odor exhibited by animals of the CON-E group was mimicked in SAM-S weanlings ( $2.125 \pm 0.31$ ) ( $p = 0.24$ ,  $t(21) = 1.197$ , comparing CON-E versus SAM-S).

Human neurobiology has shown that unilateral damage to the amygdala is sufficient to impair fear/threat conditioning (LaBar et al., 1995). Thus, histology was used to verify that the PNN-dissolving enzyme successfully reduced PNN intensity within the anterior-to-mid level of BLA of CON-E brains. Four out of the eight CON-E brains exhibited complete unilateral dissolution of PNN, such as that shown in Figure 3a, while four other CON-E brains exhibited partial unilateral dissolution of PNN. WFA labeling, reflecting labeling of PNN and the surrounding neuropil, within anterior-to-mid BLA was normalized to the value of the immediately lateral perirhinal cortex, so as to quantify the extent of enzyme dissolution, relative to the neighboring

anatomical tissue. One-way ANOVA indicated significant impact of enzyme treatment upon PNN intensity of BLA of CON tissue ( $p < .001$ ,  $F = 12.89$ ), due to significant decrease within the BLA of CON-E, relative to CON-S's (13% reduction in normalized PNN intensity,  $p < .001$ ,  $\text{mean}_{\text{CON-S}} = 1.205 \pm 0.031$ ;  $\text{mean}_{\text{CON-E}} = 1.048 \pm 0.031$ ,  $t(21) = 4.999$ ). CON-E's normalized PNN intensity was not significantly different from that of SAM-S ( $p = .0982$ ,  $\text{mean}_{\text{SAM-S}} = 1.102 \pm 0.031$ ,  $t(21) = 1.731$ ). CON-S's normalized PNN intensity was significantly different from that of SAM-S ( $p = .004$ ,  $t(21) = 3.268$ ).

### 3.6 | PV cell ontogeny in the BLA

We next sought to assess the putative impact SAM could have on developmental patterns of the BLA leading up to the weaning age by quantifying the density and intensity of immunocytochemically detected PV cells in the BLA at PN12, 15, and 18 (Figure 6). Immunolabeling of PV somata and proximal dendrites were visible in the BLA of younger animals. Two-way ANOVA of PV density across all anterior-to-posterior (AP) levels revealed a significant effect of age ( $F(2,42) = 25.21$ ,  $p < .001$ ), but not rearing condition ( $F(1,42) = 25.21$ ,  $p = .853$ ).

PN15 represented a transitional time-point for abused litters: while half of the SAM pups had PNN density that was similar to CON's (Figure 6a,b), half of the pups displayed an immature phenotype with very sparse PV labeling in the BLA (Figure 6c). Although this difference among the SAM pups yielded a trend for a SAM-vs-CON group difference at this age, the difference did not reach statistical significance ( $t(42) = 1.063$  and  $p = .293$  for PV density across all levels of BLA;  $p = .1953$  and  $t(42) = 1.316$  for the anterior-to-mid level;  $p = 0.4214$  and  $t(28) = 0.8160$  for posterior level of BLA).

Two-way ANOVA of PV density in the anterior-to-mid levels of BLA revealed age to be a significant factor [ $F(2,42) = 24.04$ ,  $p < .001$ ]

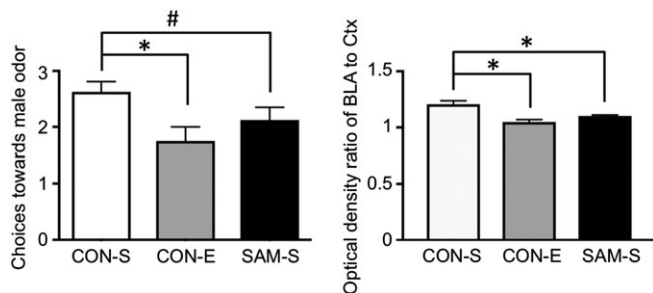


**FIGURE 5** Innate threat response of weanlings is augmented following PNN dissolution or following SAM. Chondroitinase-ABC plus hyaluronidase (ChABC+H) was infused into the BLA of CON rats at PN20 before innate threat response testing with Y-maze at PN22. Behavior was compared to age-matched saline-injected CON rats (CON-S) and saline-injected SAM (SAM-S) rats. (Panel a) Choices that CON weanlings made toward a novel male odor was significantly decreased by unilateral PNN dissolution (CON-E), compared to CON with saline infusion (CON-S) ( $N = 8$  for both groups,  $p = .01$ ) and was also marginally significantly decreased among age-matched rats that experienced SAM and received saline infusion into the BLA (SAM-S,  $N = 8$ ,  $p = .13$ ). There was no significant difference in novel male odor avoidance between the CON-E and SAM-S ( $N = 8$ ,  $p = .24$ ). WFA labeling of the BLA of the animals that underwent enzymatic dissolution of PNN were determined, using the WFA labeling in the immediately adjacent cortex to normalize the values. The normalized values (ratio of BLA to Ctx) were significantly reduced for the CON-E group, relative to CON-S. The WFA labeling of SAM-S BLAs were also significantly reduced, relative to CON-S's. Bars represent mean  $\pm$ SEM. Asterisks indicate  $p < .05$ ; # indicates  $.05 < p < .1$

but not the rearing condition [ $F(1,42) = .1443$ ,  $p = .706$ ], with no interaction between age and the rearing conditions [ $F(2,42) = 1.190$ ,  $p = .314$ ]. Fisher's post hoc analysis revealed a robust increase in the anterior-to-mid level BLA of pups reared under the control condition from PN12 to PN15 (10-fold;  $t(42) = 3.763$ ,  $p < .001$ ), with no further significant increase from PN15 to PN18 ( $t(42) = 0.504$ ,  $p = .617$ ) or from PN18 to PN23 ( $p = .84$ ,  $t(56) = .3744$ ).

The posterior levels of the BLA also showed a main effect of age [ $F(2,28) = 16.03$ ,  $p < .001$ ], but not of treatment [ $F(1,28) = 0.339$ ,  $p = .565$ ] and no interaction between age and treatment [ $F(2,28) = 0.202$ ,  $p = .818$ ]. PV cell density in the posterior BLA of the CON group of animals increased with a delay, as compared to the developmental changes observed among the CON groups in ant-to-mid level of BLA (Figure 6d). PV cells, absent in five out of the eight CON animals at PN12, increased 19-fold by PN15 and by 250% more by PN18 ( $t(28) = 2.594$ ,  $p = .015$ ). PV cell density in the posterior BLA plateaued beyond PN18, as there was no further increase from PN18 to PN23 ( $p = .88$ ,  $t(39) = 0.1545$ ).

In the anterior-to-mid level BLA of the SAM group, PV cell density increased but with a delay, compared to the CON group, as the plateau was attained by PN15 for the CON group but was not attained until PN18 for the SAM group (Figure 6d). The SAM group showed an eightfold increase from PN12 to PN15 ( $t(42) = 2.664$ ,  $p = .029$ ) and another 90% increase from PN15 to PN18 ( $t(42) = 2.79$ ,  $p = .021$ ). In the posterior BLA, the developmental change was similar between the CON and SAM, as both groups attained plateau at around PN18.

The intensity of PV cell labeling was almost completely unchanged during the pre-weaning ages, whether reared under normal or SAM condition (effect of age for all anterior-to-posterior levels  $F(2,34) = 1.404$ ,  $p < .260$ ; effect of age for anterior-to-mid level  $F(2,34) = 1.379$ ,  $p < .266$ ; effect of age for the posterior level  $F(2,17) = 0.383$ ,  $p = .688$ ; two-way ANOVA); Figure 6e). This indicated that the dramatic ontogenetic changes in PV density (Figure 6d) are unlikely to have been due to failures in detecting PV labeling. Two-way ANOVA did revealed a trend toward a treatment group effect in the posterior BLA (effect of treatment for all anterior-to-posterior levels  $F(1,34) = 2.257$ ,  $p = .142$ ; effect of treatment for anterior-to-mid level  $F(1,34) = 1.631$ ,  $p = .210$ ; effect of treatment for the posterior level  $F(1,17) = 0.592$ ,  $p = .075$ ; Figure 6e). While the negative outcome of the two-way ANOVA precludes further post hoc analysis of the treatment effect, there was significant reduction of PV intensity within SAM brains at a single time point of PN12 within the posterior BLA by 42% ( $t(17) = 2.672$ ,  $p = .016$ ).

### 3.7 | PNN ontogeny in the BLA

Having observed that SAM reduced PNN intensity in the anterior-to-mid BLA but not in the posterior BLA at PN23, we asked whether this difference at PN23 reflects a difference in developmental trajectory of PNNs during the post-SAM pre-weaning ages. To answer this question, we analyzed PNN density and intensity at PN12, PN15, and PN18 (Figure 7). In agreement with previous studies (Horii-Hayashi et al., 2015), PNN labeling around somata ranged from more diffuse to darker and more defined around both somata and proximal dendrites (Figure 7a). There was also diffuse proteoglycan labeling that did not cluster around individual somata, which were categorized as labeling in the neuropil surrounding the PNN.

Two-way ANOVA of PNN density (Figure 7b) revealed a strong age-effect (effect of age for all anterior-to-posterior levels  $F(2,30) = 7.029$ ,  $p = .003$ ; effect of age for anterior-to-mid level  $F(2,30) = 7.741$ ,  $p < .002$ ; effect of age for the posterior level  $F(1,17) = 0.592$ ,  $p = .028$ ), as well as a rearing effect in anterior/mid and combined anterior-to-posterior levels, but only marginally in posterior levels (effect of rearing for all anterior-to-posterior levels  $F(1,30) = 4.226$ ,  $p = .049$ ; effect of treatment for anterior-to-mid level  $F(1,30) = 5.084$ ,  $p = .032$ ; effect of treatment for the posterior level  $F(1,20) = 0.1118$ ,  $p = .742$ ) and no interaction between the factors of age and rearing. Post hoc analyses of the rearing effect in anterior-to-mid level BLA and anterior-to-posterior levels did not yield significance, although we did observe a strong trend toward reduction of PNN density within SAM brains at a single time point of PN15 ( $t(30) = 1.981$ ,  $p = .0568$  for anterior-to-mid level and  $t(30) = 1.907$ ,  $p = .066$  in all anterior-to-posterior levels).

For both the CON and SAM groups, Fisher's post hoc analysis of the age effect revealed robust increases in PNN density in the anterior-mid level BLA from PN12 to PN18 ( $t(30) = 2.965$ ,  $p = .006$ , 2.6-fold increase for CON;  $t(30) = 2.501$ ,  $p = .018$ , sixfold increase for SAM; Figure 7b). Among the CON groups, the posterior BLA exhibited levels of PNN density that were significantly less than seen at PN23 ( $p < .0001$  for CON tissue, compared to values at PN12, PN15, or

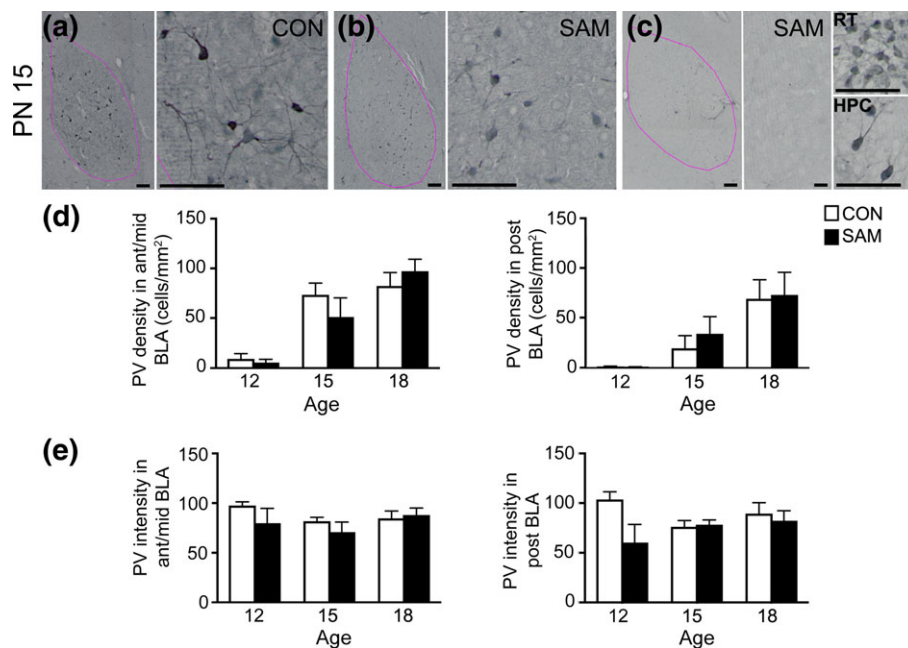


**FIGURE 6** PV ontogeny in the BLA. PV cells were examined in the BLA of SAM and CON rats at PN12, PN15, and PN18. The left sides of panels a, b, and c depict contour of the BLA in pink, which is distinguishable by the high density of PV immunoreactivity, in addition to the landmarks of the central amygdala medially, the lateral amygdala dorsally, and the external capsule laterally (scale bars = 100  $\mu$ m). All panels were taken at a magnification of 10 $\times$ . Scale bars in first panel = 200  $\mu$ m and apply to all subsequent whole BLA images; scale bars for the micrographs to the right of each panel = 20  $\mu$ m. All of these micrographs were taken from the BLA of PN15 animals. PN15 represents a transitional time-point for abused litters: while half of the SAM pups (panel b) had PNN density that was similar to CON's (panel a), half of the pups displayed an immature phenotype with very sparse PV+ labeling in the BLA (panel c). Prominent PV+ labeling in the reticular thalamus (RT, top right) and dorsal hippocampus (HPC, bottom right) confirms reduction in PV+ cell density is specific to the BLA. (Panels d, e) The graphs show developmental changes in PV density (panel d) and PV intensity (panel e) of CON and SAM brains during pre-weaning ages, separately for anterior-to-mid (left graph) and posterior (right graph) levels of BLA. Bars represent mean and SEM. The small alphabets above the bars depict the following: a = significantly different from PN12 within the same rearing group; b = significantly different from PN15 within the same rearing group. PV intensity increased significantly from PN12 for the posterior BLA of the SAM group. CON groups exhibited no remarkable change in PV intensity across the pre-weaning ages. Neither the density nor intensity of PV labeling was detectably altered by SAM treatment. # indicates .05 <  $p$  < .1 for comparison across the early life treatment groups [Color figure can be viewed at [wileyonlinelibrary.com](http://wileyonlinelibrary.com)]

PN18,  $t(27) = 6.662, 5.788, 4.578$ , respectively). Similarly, among the SAM groups, the posterior BLA exhibited levels of PNN density that were significantly less than seen at PN23 (Figure 4) ( $p < .01$  for SAM tissue, compared to values at PN12, 15, or 18,  $t(27) = 4.172, 3.047$ , and 2.956, respectively).

Two-way ANOVA of the intensity of PNN labeling (Figure 6c) revealed no significant effect of rearing condition (all anterior-to-posterior levels:  $F(1,27) < 0.001$ ,  $p = .983$ ; anterior-to-mid level BLA:  $F(1,27) < 0.001$ ,  $p = .977$ ; posterior level BLA:  $F(1,15) = 0.005$ ,  $p = .945$ ) and no significant effect of age (all anterior-to-posterior levels:  $F(2,27) = 0.265$ ,  $p = .769$ ; anterior-to-mid level BLA:  $F(2,27) = 0.528$ ,  $p = .977$ ; posterior level BLA:  $F(2,15) = 2.394$ ,  $p = .125$ ) and no interaction between age and rearing. The ontogenetic analysis revealed that the reduced PNN intensity in the anterior-to-mid level BLA of the SAM group that was noted at single time point of PN23 ( $t(37) = 2.291$ ,  $p = .0278$ , Figure 5c) was due to a significant decrease from an earlier time point of PN18 (20%,  $t(37) = 3.208$ ,  $p = .0028$ ).

Intensity of the neuropil surrounding PNNs did not differ significantly across the ages or across the two rearing groups at any level of the BLA.

### 3.8 | EM quantification of PV innervation of neuronal cell bodies in the BLA

Does SAM induce hyperexcitability of the amygdala through perturbation of PV-inhibition of pyramidal cells? This question was addressed by quantitative electron microscopic analysis of axo-somatic inhibitory synapses formed by PV-immunoreactive axon terminals onto pyramidal cells. EM analysis was chosen to be in the anterior-to-mid level of BLA, where reduction of PNN intensity was detected within brains of SAM animals.

As was previously observed (Smith, Pare, & Pare, 1998, 2000), intense PV-immunolabeling was detected within a subpopulation of axon terminals forming axo-somatic axon terminals (Figures 8 and 9). PV-immunolabeling was also readily apparent within perikaryal cytoplasm of cell bodies with deep indentations of the nuclear envelope (Figure 9).

Quantitative analysis revealed group differences in axo-somatic contacts formed by PV terminals onto pyramidal cell bodies (Figure 8a-c). The percentage of pyramidal cell bodies' plasma membrane receiving input from PV terminals was 27% less in the BLA of SAM brains, relative to CONs' ( $p = .0487$ ,  $t(118) = 1.992$ ; Figure 8d). This was due primarily to a 24% reduction in the frequency of

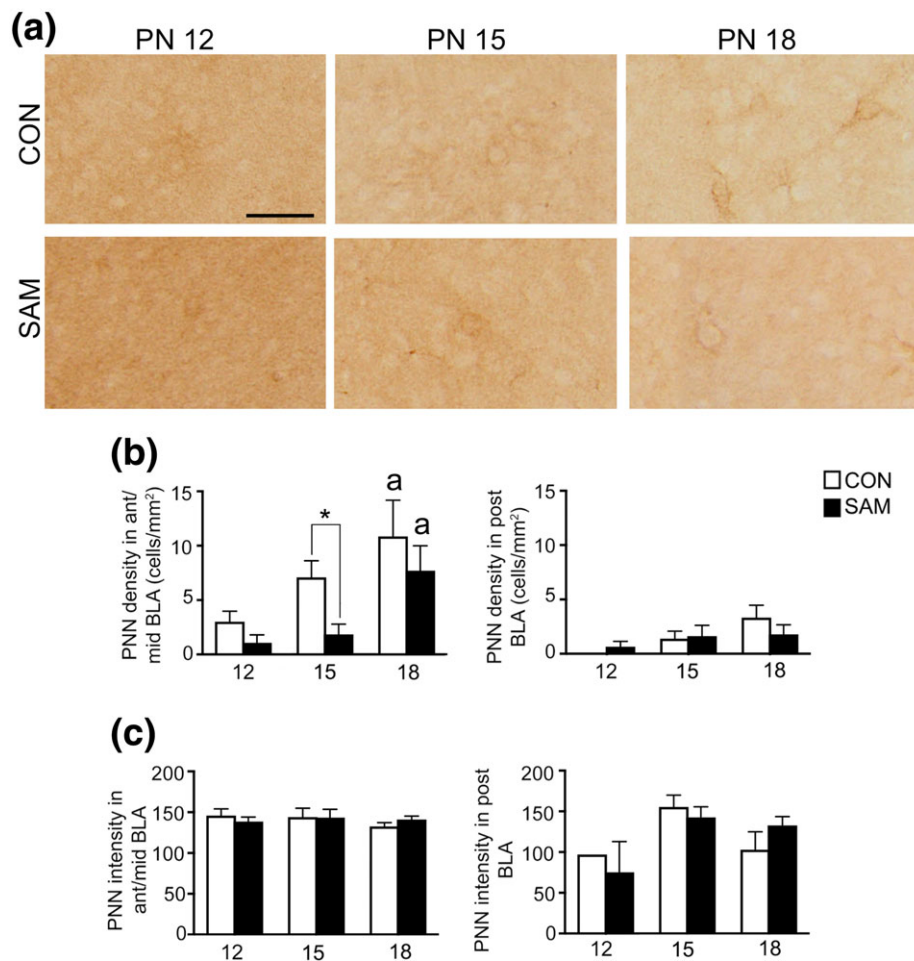


**FIGURE 7** PNN ontogeny in the BLA. (Panel a) PNN cells were examined in the BLA of SAM and CON rats at PN12, PN15, and PN18. Micrographs show details of sample PNNs. All panels were taken at a magnification of 10x. Scale bar = 20 μm and applies to all panels). (Panels b,c) The graphs show developmental changes in PNN density (panel b) and PNN intensity (panel c) of CON and SAM brains during pre-weaning ages, separately for anterior-to-mid (left graph) and posterior (right graph) levels of BLA. Bars represent mean and SEM. In ant/mid BLA, PNN cell density was transiently reduced by SAM at PN15. In posterior BLA, PNN cell density was not reduced at younger ages, as was observed at PN23 (Figure 4). PNN density rises during pre-weaning ages, reaching a plateau at PN18 for CON brains but not yet plateaued at this age for SAM brains at anterior-to-mid levels. # in (panel b) represents significant rearing effects at a particular age ( $p = .032$ ), even though two-way ANOVA indicated a  $p$ -value  $>.05$ . The small alphabets above the bars depict significant differences between age groups within the same rearing condition with: a = significantly different from PN12; b = significantly different from PN15; c = significantly different from PN18 [Color figure can be viewed at [wileyonlinelibrary.com](http://wileyonlinelibrary.com)]

contacts formed by PV terminals onto pyramidal cell bodies, per μm of plasma membrane sampled (Figure 8e;  $p = .0458$ ,  $t(118) = 2.018$ , comparing SAM versus CON) but also a significant reduction in the average length of synaptic contacts formed by PV terminals (Figure 8f; 13% reduction,  $p = .0293$ ,  $t(106) = 2.209$ ).

PV terminals forming axo-somatic contacts onto PV cells were similarly diminished (Figure 9). The percentage of PV cell bodies' plasma membrane receiving input from PV terminals was reduced by 54% in the BLA of SAM brains ( $p < .0001$ ,  $t(118) = 3.513$ ; Figure 9d). This was due primarily to a 51% reduction in the frequency of PV terminal contacts onto the cell bodies of PV cells ( $p < .001$ ,  $t(118) = 3.549$ ; Figure 9e), rather than changes in PV terminal lengths ( $p = .35$ , Figure 9f).

Excitatory asymmetric terminal (AT) innervation onto PV somata was also assessed by EM (Figure 9c). While there was no CON versus SAM difference in the percentage of PV cell bodies' plasma membrane

receiving excitatory input from ATs ( $p = .96$ ; Figure 9d), there was a significant 25% increase in average AT lengths onto PV cells in the BLA of the SAM group ( $p = .0323$ ,  $t(87) = 2.175$ , Figure 9f) and a trend for a 20% decrease in the frequency of ATs forming excitatory synapses onto the cell bodies of PV cells ( $p = .18$ , Figure 9e).

In summary, these EM data indicate that SAM reduces synaptic inhibition exerted by PV neurons in the BLA without a significant change in the excitatory drive onto PV neurons.

## 4 | DISCUSSION

We show that maternal maltreatment induced by SAM during early life generates heightened innate threat response and reduction of PV-mediated inhibitory synapses of the BLA at weaning age, just as pups are beginning to gain independence from the mother. We also show



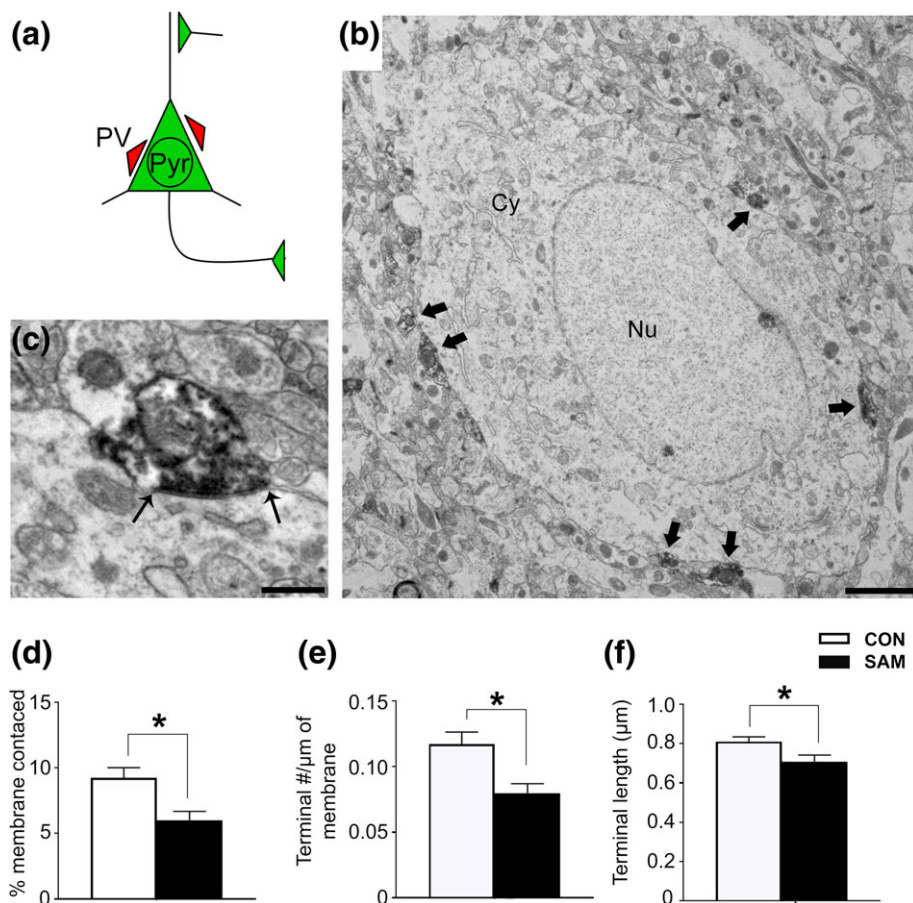


**FIGURE 8** Electron microscopy of PV-to-pyramidal contacts. (Panel a) Schematic of a BLA pyramidal cell. PV terminals innervate pyramidal cells at the soma and proximal dendrite, whereas excitatory inputs contact pyramidal cells at dendritic spines. (Panel b) Electron micrograph of a pyramidal cell with PV terminal contacts indicated with black arrows. Pyramidal cells were distinguished from nonPV interneurons by two features characteristic of pyramidal cells: The smooth nuclear envelope and lack of axo-somatic asymmetric synapses with thick post-synaptic densities (PSDs). (Panel c) Enlarged micrograph of a PV terminal contacting the plasma membrane of a pyramidal cell. Black arrows indicate the length of the terminal. Synaptic contact is confirmed by the plasma membrane of the pyramidal cell that forms a parallel alignment with the plasma membrane of the PV terminal. (Panel d) The percentage of pyramidal membrane receiving input from PV terminals was less for the SAMs' BLAs, relative to CONs'. (Panel e) The frequency of synaptic contacts by PV terminals onto pyramidal cells was less for the SAM rats, relative to CONs'. (Panel f) Average lengths of PV terminal contacts were also significantly different between groups. Bar graphs depict mean values and SEM. Asterisk indicates  $p < .05$  [Color figure can be viewed at [wileyonlinelibrary.com](http://wileyonlinelibrary.com)]

that unilateral PNN depletion within the BLA converts the threat response of normally reared animals to become abnormally high, as we've shown among weanlings with a history of early life maltreatment. Since PNN dissolution reduces excitability of PV cells (Balmer, 2016), this third finding strengthens a causal link between reduction of PV-mediated synaptic inhibition in the BLA and heightened innate threat response. Future studies that experimentally reduce PV-mediated synaptic inhibition in the BLA while measuring innate threat response would be able to solidify this causal link further. Localized lesion of the BLA subnucleus reduces predator odor threat response (Takahashi et al., 2007). Since the animals receiving the enzymatic treatment to dissolve PNN did not exhibit reduction of threat response but, instead, heightened threat responses, it is likely that the enzymatic treatment with the micropipette left the BLA intact. This was verified by Nissl staining of the enzymatically treated BLA.

We observed a strikingly strong correlation ( $R = -0.9$ ) between PV cell density in the anterior-to-mid level BLA and innate threat responsiveness at weaning of normally reared animals: this correlation

was lost within brains of animals that had experienced maternal maltreatment. Apparently, SAM diminishes the involvement of these PV neurons in suppression of BLA excitability and threat response. This diminished influence by PV neurons could be explained, in part, by the reduction of PNN in the anterior-to-mid level BLA of maltreated animals at weaning age, which is expected to weaken excitability of inhibition by PV cells (Balmer, 2016). This, together with the reduction of PV-innervation onto pyramidal cells, provides anatomical support for the idea that reduction of PV/PNN-mediated inhibition in the anterior-to-mid level BLA causes hyperexcitability of the BLA, which, in turn, elevates innate threat responsiveness of weanlings (Figure 10).

#### 4.1 | Signatures of resilience

SAM induced a reduction of PV intensity in the posterior BLA but only transiently at PN12. In the hippocampus of adult mice, Donato, Chowdhury, Lahr, and Caroni (2015) describe a transient reduction in

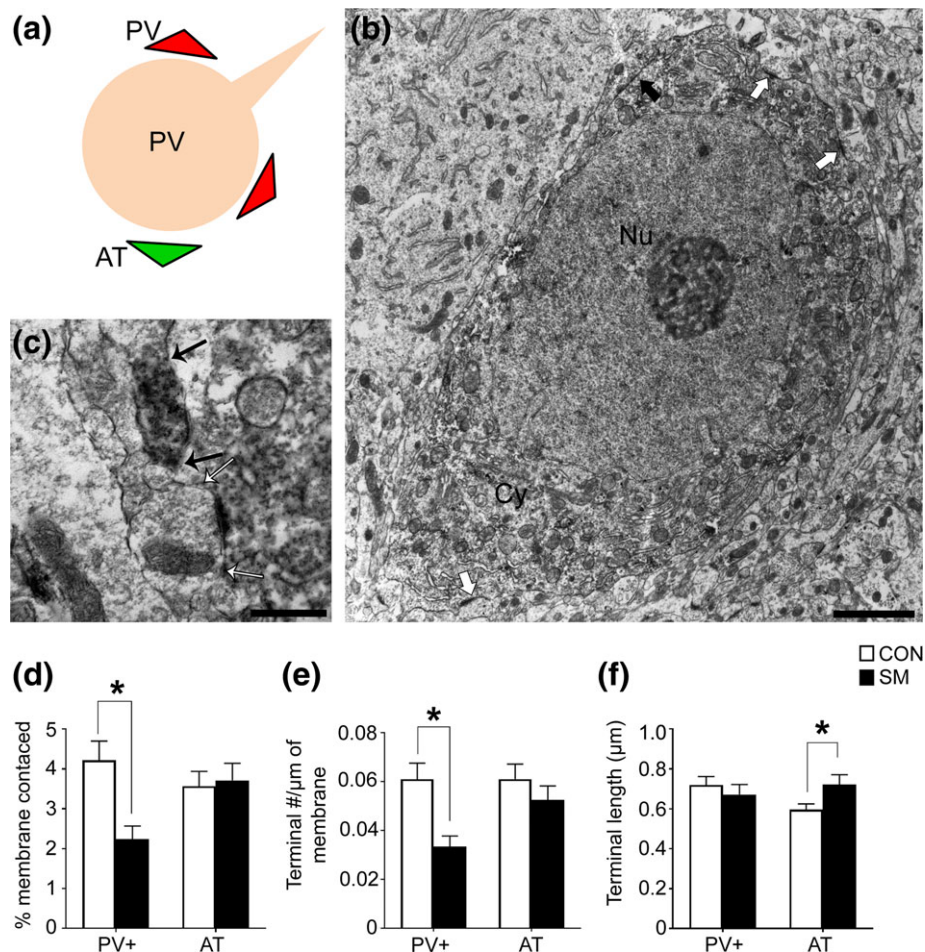


**FIGURE 9** Electron microscopy of PV and excitatory synaptic contacts onto PV cell bodies. (Panel a) Schematic of BLA PV cell body innervated by PV terminals (red triangles) and asymmetric excitatory axon terminals (AT, green triangles). (Panel b) Electron micrograph of a DAB-labeled PV cell body with PV terminal contacts indicated with black arrows. PV cells were distinguished from pyramidal cells by two features characteristic of PV cells: Invaginated nuclear envelope (white arrowheads) and presence of axo-somatic asymmetric synapses with thick post-synaptic densities (white arrows). (Panel c) Enlarged micrograph of a PV terminal contacting the plasma membrane of another PV cell body. A black arrow indicates the border between the PV cell body's plasma membrane and the PV terminal. (Panel d) The percentage of PV cell membrane receiving input from PV terminals and ATs. Only PV+ terminal innervation was reduced by SAM. (Panel e) PV terminal and AT frequency per unit length of PV cell's plasma membrane. SAM reduced the frequency of PV terminal number without a significant change in the frequency of AT number. (Panel f) Average of the lengths of PV terminals forming synaptic contacts to PV cell bodies length was not different between the two rearing groups but the average lengths of ATs were significantly increased for the SAM group. Bar graphs depict mean values and SEM. Asterisks indicate  $p < .05$  [Color figure can be viewed at [wileyonlinelibrary.com](http://wileyonlinelibrary.com)]

PV intensity that promotes increased plasticity via reduced inhibition of pyramidal cells. A similar mechanism may be at play in the developing BLA for individuals recovering from early life trauma, transiently extending the period of postnatal plasticity.

Reduction of BLA PNN density in the anterior-to-mid level BLA during the pre-weaning phase of development is transient and becomes normalized by weaning age. In addition, reduction of PV intensity in the posterior BLA that is evident immediately following SAM becomes normalized within three days. These SAM-related cellular events occur within the context of profound ontogenetic changes that take place normally during the pre-weaning period, whereby PV and PNN cell densities increase four to tenfold. These new findings complement recent results showing continued maturation of PV and PNN in normative development from PN24 to adulthood (Baker et al., 2017) and the potential for continued impact of developmental insults and recovery from them.

## 4.2 | Functional significance of the reduced PV-to-pyramidal innervation

Pyramidal projecting from the BLA to the central nucleus of the amygdala (CeA) has been identified as a major contributor to the production of anxiety-like behavior (Tye et al., 2011): when axon terminals of pyramidal cells within the CeA are optogenetically stimulated, anxiolysis is generated. However, when pyramidal cells are optogenetically evoked to fire somatically, anxiolysis is not elicited. This latter effect could be due to recruitment of antagonistic structures that are extrinsic to the BLA (Janak & Tye, 2015; Roozendaal, McEwen, & Chattarji, 2009) but also due to the recruitment of antagonistic circuit intrinsic to the BLA, involving PV cells that generate feedback inhibition (Ryan et al., 2012; Woodruff & Sah, 2007a, 2007b). A PV cell can inhibit a synaptically connected pyramidal cell with a single action potential (Woodruff & Sah, 2007a). Thus, there is ample evidence to support

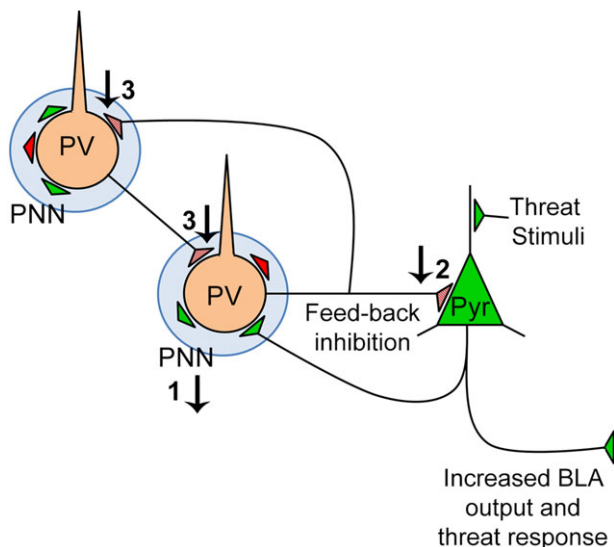


**FIGURE 10** Schematic of BLA circuitry at weaning. Maternal maltreatment in early life impacts PV circuitry: (1) PNN intensity is reduced, which in turn suppresses PV function; (2) PV-to-Pyr innervation is reduced, thus lessening inhibition of Pyr cells; (3) PV-to-PV innervation is reduced, thus diminishing the powerful synchrony of BLA inhibition by PV cells. These changes could increase threat response by increasing pyramidal cell excitability [Color figure can be viewed at [wileyonlinelibrary.com](http://wileyonlinelibrary.com)]

the idea that reduction of PV inhibition in the BLA, which we observed, contributes to hyperexcitability of the amygdala following maternal abuse (Dube et al., 2015) and heightened innate threat response that we observed. Hyperexcitability of the pyramidal cells in the BLA is likely to also contribute to heightened anxiety-like behavior that reduces social behavior (Felix-Ortiz & Tye, 2014).

### 4.3 | Functional significance of the reduced PV-to-PV innervation

While PV neurons in the BLA form dendritic and axonal electrical synapses, the majority of PV-to-PV synapses are axo-somatic (Muller, Mascagni, & McDonald, 2005, 2006). Of them, large PV+ terminals ( $>1 \mu\text{m}^2$ ) are associated with PV+ projections from the basal forebrain (Muller et al., 2005). Cumulative histogram of PV terminal lengths indicated no change in the frequency of PV terminal of any size range following SAM, relative to CON (data not shown). Thus, PV terminals of both extrinsic and local are likely to have been reduced by SAM.

Reduced PV-to-PV innervation would contribute to decreased BLA activity, but apparently, this was not sufficient to normalize hyperexcitability arising from the reduced PV-to-pyramidal innervation, since SAM animals still exhibited elevated threat response. Disinhibition via PV innervation of somatostatin+ cells which, in turn, contact dendrites of pyramidal cells, drive BLA fear/threat learning (Wolff et al., 2014). The effects of early life trauma on this form of BLA disinhibition remain to be explored.

Reduced PV-to-PV innervation may also contribute to reduced oscillatory power in the high frequency gamma range, which has been shown to require synchronous PV cell activity in the BLA (Ryan et al., 2012). Specifically, PV cells coordinate spike timing of Pyr cells, to

entrain high frequency oscillations in the BLA (Ryan et al., 2012). Gamma activity increases with PV cell development (Yang et al., 2015) and may be a critical component to functional theta-gamma coupling between prefrontal cortex and BLA, which has been shown to be necessary for processing safety signals (Stujenske, Likhtik, Topiwala, & Gordon, 2014).

### 4.4 | AT onto PV somata are longer in the BLA of SAM brains

Excitatory terminals onto PV somata were, on average, longer in the BLA of SAM brains. These excitatory axo-somatic synapses are more likely to be of local origin than from cortex (Duvarci & Pare, 2014). This increase may correlate with an increase in AMPA receptor number per synapse, as has been shown for the hippocampus and cortex (Kharazia & Weinberg, 1999; Nusser et al., 1998). Since the number of ATs onto PV somata is less for SAM, this would indicate that BLA of SAM brains are driven more strongly but by fewer sources. Such a change may underlie reduced flexibility in animals' responsiveness to threatening stimuli.

### 4.5 | Functional significance of the reduced PNN intensity in the anterior-to-mid level BLA

Early life trauma induced increase in threat response of weanlings and reduction of PNN intensity in the BLA. Conversely, CON weanlings that were free of early life trauma also showed increase in threat response following enzymatic dissolution of PNN proteoglycans in the BLA two days prior. Since the great majority of PNNs surround PV neurons in the BLA of PN23 rats, these findings strengthen the causal link between PNN-supported PV-inhibition of BLA and suppression of threat response.

The reduction of PNN intensity at weaning was evident for the anterior-to-mid level BLA but not for the posterior BLA. It has recently become evident that PNN in the BLA of postnatal week 5–10 male mice encapsulate PV neurons in the anterior BLA but more of the excitatory neurons in the posterior BLA (Morikawa et al., 2017). Data we obtained from dual PNN-PV labeling indicate that, at least at PN23, the great majority of PNNs (89%) surround PV cells at anterior, mid, and posterior sectors of BLA of both males and females. This observation confirms Baker's report regarding BLA at mid-level in PN24 rats (Baker et al., 2017). Whether PNNs in the BLA of rats exhibit differences along the anterior–posterior axis in terms of the cell types that they enwrap and whether this pattern evolves during adolescence and into adulthood for males or females deserves to be examined more closely. Nevertheless, based on our observations, we conclude that neurons with reduced PNN intensity following SAM are likely to have affected PV cells much more (approximately nine-times more) than excitatory neurons.

PNN intensity is frequently used as a proxy for maturity (Carulli, Foscarin, Faralli, Pajaj, & Rossi, 2013; Chen, He, & Lasek, 2015; Foscarin et al., 2011; Happel & Frischknecht, 2016; Slaker et al., 2015; Vazquez-Sanroman, Monje, & Bardo, 2017). Thus, the lighter intensity of SAM brains' PNN at PN23 could also indicate reduced PNN maturity. Future studies that detect the maturational transition of PNN's



molecular structure from chondroitin 6-sulfation (C6S) to C4S, which is associated with reduction of plasticity (Miyata, Komatsu, Yoshimura, Taya, & Kitagawa, 2012) would be valuable for gaining further insight into the impact of the reduced PNN intensity following SAM.

Hippocampal PNNs regulate plasticity at axo-somatic excitatory inputs to PV cells by increasing AMPA receptor localization at the synapse via expression of brevican (Favuzzi et al., 2017). In addition, PNNs have been shown to protect the cells that they envelop from oxidative stress (Cabungcal et al., 2013; Suttikus et al., 2014). Peri-weaning PV cells in the BLA of SAM weanlings may also be more prone to oxidative stress, and exhibit reduced plasticity at excitatory synaptic inputs. Since disruption of GABAergic development broadens tuning curves responsible for adaptive response to stimuli (Isaacson & Scanziani, 2011), BLA tuning to threat may also be broadened for SAM rats, as animals develop heightened awareness of potential threats under conditions of resource scarcity.

## 5 | CONCLUSIONS

The present results provide an anatomical mechanism for early life SAM maltreatment-induced heightened behavioral and amygdala responses of infants to threat (Perry et al., 2016) by demonstrating enduring amygdala synaptic changes. SAM treatment ends just as BLA cells are beginning to express PV and PNN in normal ontogeny (PN12). This indicates that reductions of PV synapse lengths, PNN density, and PNN intensity observed at pre- and peri-weaning age do not result simply from suppression of PV- or PNN-protein expression during the SAM treatment. Rather, the SAM effects we observe at PN23 are the delayed manifestation of SAM, presumably resulting from perturbations in BLA circuitry that exist during SAM, which alter the developmental trajectory of the activity-dependent emergence of PV-synapses and PNNs during the pre-weaning ages that follow SAM. Further studies are needed to determine whether the cellular changes in the BLA at weaning persists through adolescence and into adulthood to support the dynamic changes in the threat system, including the decreasing threat responses seen in adults following early life trauma, SAM (Moriceau, Raineki, Holman, Holman, & Sullivan, 2009; Perry et al., in revision).

Unlike the pups that experience longer, more severe durations of SAM (Dube et al., 2015), none of the animals in our study exhibited weight loss or spasms related to limbic epileptic seizures. This indicates that changes evoked by SAM can be enduring and synaptic, even for individuals that have experienced milder forms of maternal abuse. The SAM infant manipulation's moderate maternal maltreatment, which is induced by a reduction in environmental resources, provides pups with nutritional needs within a sanitary environment, and potentially models early life stress-induced compromised parenting sometimes seen in impoverished environments (Perry et al., 2018). It is well documented that poverty during a child's early neurodevelopment puts that child at long-term risk of developing a psychiatric illness (Johnson, Riis, & Noble, 2016). The brain is shaped by the environment and continues to develop through adolescence (Aoki, Chowdhury, Wable, & Chen, 2017; Casey & Lee, 2015; Giedd et al.,

1999), including amygdala of children and rodents (Pattwell et al., 2012).

It is possible that the abnormally high innate threat response at weaning age leads to secondary social behavioral abnormalities during adolescence, affecting developmental trajectory of a wider net of brain structures underlying social behavior. Studies are underway to determine whether the cellular changes in the BLA at weaning persists through adolescence and whether normalization of social experience during adolescence can promote normalization of BLA synapses and brain structures extrinsic to the BLA.

## ACKNOWLEDGMENTS

This study was supported by a grant from National Institute of Mental Health [R37HD083217 (RMS)] and National Institutes of Health [F32MH112232 (MO), F31 MH112372 (AS), R21MH105846 (CA)]. Authors thank Yi-Wen Chen for her critique of the manuscript and assistance with statistical analyses. They also thank Claudia Farb for her advice regarding PV immunocytochemistry. Authors also thank Sabrina George, Ishan Handa, and Sarah Martin for their help with histological procedures.

## ORCID

Adrienne N. Santiago  <https://orcid.org/0000-0002-5022-1675>

Chiye Aoki  <https://orcid.org/0000-0003-4010-9425>

## REFERENCES

- Aoki, C., Chowdhury, T. G., Wable, G. S., & Chen, Y. W. (2017). Synaptic changes in the hippocampus of adolescent female rodents associated with resilience to anxiety and suppression of food restriction-evoked hyperactivity in an animal model for anorexia nervosa. *Brain Research*, 1654(Part B), 102–115.
- Aoki, C., & Erisir, A. (2013). Experience-dependent synaptic plasticity in the developing cerebral cortex. In V. Pickel & M. Segal (Eds.), *The synapse: Structure and function* (Vol. 3, pp. 397–420). Academic Press. [www.neuroscience.com](http://www.neuroscience.com).
- Aoki, C., Rodrigues, S., & Kurose, H. (2000). Use of electron microscopy in the detection of adrenergic receptors. *Methods in Molecular Biology*, 126, 535–563.
- Baker, K. D., Gray, A. R., & Richardson, R. (2017). The development of perineuronal nets around parvalbumin gabaergic neurons in the medial prefrontal cortex and basolateral amygdala of rats. *Behavioral Neuroscience*, 131(4), 289–303.
- Balmer, T. S. (2016). Perineuronal nets enhance the excitability of fast-spiking neurons. *eNeuro*, 3(4), 1–13.
- Berdel, B., & Morys, J. (2000). Expression of calbindin-D28k and parvalbumin during development of rat's basolateral amygdaloid complex. *International Journal of Developmental Neuroscience*, 18(6), 501–513.
- Cabungcal, J. H., Steullet, P., Morishita, H., Kraftsik, R., Cuenod, M., Hensch, T. K., & Do, K. Q. (2013). Perineuronal nets protect fast-spiking interneurons against oxidative stress. *Proceedings of the National Academy of Sciences of the United States of America*, 110(22), 9130–9135.
- Callaghan, B. L., Sullivan, R. M., Howell, B., & Tottenham, N. (2014). The international society for developmental psychobiology Sackler symposium: Early adversity and the maturation of emotion circuits—A cross-species analysis. *Developmental Psychobiology*, 56(8), 1635–1650.
- Carulli, D., Foscarin, S., Faralli, A., Pajaj, E., & Rossi, F. (2013). Modulation of semaphorin3A in perineuronal nets during structural plasticity in the adult cerebellum. *Molecular and Cellular Neuroscience*, 57, 10–22.



- Casey, B. J., & Lee, F. S. (2015). Optimizing treatments for anxiety by age and genetics. *Annals of the New York Academy of Sciences*, 1345, 16–24.
- Celio, M. R., & Heizmann, C. W. (1981). Calcium-binding protein parvalbumin as a neuronal marker. *Nature*, 293(5830), 300–302.
- Chen, H., He, D., & Lasek, A. W. (2015). Repeated binge drinking increases perineuronal nets in the insular cortex. *Alcoholism: Clinical and Experimental Research*, 39(10), 1930–1938.
- Donato, F., Chowdhury, A., Lahr, M., & Caroni, P. (2015). Early- and late-born parvalbumin basket cell subpopulations exhibiting distinct regulation and roles in learning. *Neuron*, 85(4), 770–786.
- Drury, S. S., Sanchez, M. M., & Gonzalez, A. (2015). When mothering goes awry: Challenges and opportunities for utilizing evidence across rodent, nonhuman primate and human studies to better define the biological consequences of negative early caregiving. *Hormones and Behavior*, 77, 182–192.
- Dube, C. M., Molet, J., Singh-Taylor, A., Ivy, A., Maras, P. M., & Baram, T. Z. (2015). Hyper-excitability and epilepsy generated by chronic early-life stress. *Neurobiology of Stress*, 2, 10–19.
- Duvarci, S., & Pare, D. (2014). Amygdala microcircuits controlling learned fear. *Neuron*, 82(5), 966–980.
- Farb, C. R., Aoki, C., & Ledoux, J. E. (1995). Differential localization of NMDA and AMPA receptor subunits in the lateral and basal nuclei of the amygdala: A light and electron microscopic study. *Journal of Comparative Neurology*, 362(1), 86–108.
- Fareri, D. S., & Tottenham, N. (2016). Effects of early life stress on amygdala and striatal development. *Developmental Cognitive Neuroscience*, 19, 233–247.
- Favuzzi, E., Marques-Smith, A., Deogracias, R., Winterflood, C. M., Sánchez-Aguilera, A., Mantoan, L., ... Rico, B. (2017). Activity-dependent gating of Parvalbumin interneuron function by the Perineuronal net protein Brevican. *Neuron*, 95(3), 639–655. e610.
- Felix-Ortiz, A. C., & Tye, K. M. (2014). Amygdala inputs to the ventral hippocampus bidirectionally modulate social behavior. *Journal of Neuroscience*, 34(2), 586–595.
- Fitzgerald, M. L., Chan, J., Mackie, K., Lupica, C. R., & Pickel, V. M. (2012). Altered dendritic distribution of dopamine D2 receptors and reduction in mitochondrial number in parvalbumin-containing interneurons in the medial prefrontal cortex of cannabinoid-1 (CB1) receptor knockout mice. *Journal of Comparative Neurology*, 520(17), 4013–4031.
- Foscarin, S., Ponzione, D., Pajaj, E., Leto, K., Gawlak, M., Wilczynski, G. M., ... Carulli, D. (2011). Experience-dependent plasticity and modulation of growth regulatory molecules at central synapses. *PLoS One*, 6(1), e16666.
- Giedd, J. N., Blumenthal, J., Jeffries, N. O., Castellanos, F. X., Liu, H., Zijdenbos, A., ... Rapoport, J. L. (1999). Brain development during childhood and adolescence: A longitudinal MRI study. *Nature Neuroscience*, 2(10), 861–863.
- Gogolla, N., Caroni, P., Luthi, A., & Herry, C. (2009). Perineuronal nets protect fear memories from erasure. *Science*, 325(5945), 1258–1261.
- Gunnar, M. R., Hostinar, C. E., Sanchez, M. M., Tottenham, N., & Sullivan, R. M. (2015). Parental buffering of fear and stress neurobiology: Reviewing parallels across rodent, monkey, and human models. *Social Neuroscience*, 10(5), 474–478.
- Hackney, C. M., Mahendrasingam, S., Penn, A., & Fettiplace, R. (2005). The concentrations of calcium buffering proteins in mammalian cochlear hair cells. *Journal of Neuroscience*, 25(34), 7867–7875.
- Hane, A. A., & Fox, N. A. (2016). Early caregiving and human biobehavioral development: A comparative physiology approach. *Current Opinion in Behavioral Sciences*, 7, 82–90.
- Happel, M. F., & Frischknecht, R. (2016). Neuronal plasticity in the juvenile and adult brain regulated by the extracellular matrix. *Composition and function of the extracellular matrix in the human body*. Francesco Travascio, IntechOpen, 143–158. doi:10.5772/62452. Available from: <https://www.intechopen.com/books/composition-and-function-of-the-extracellular-matrix-in-the-human-body/neuronal-plasticity-in-the-juvenile-and-adult-brain-regulated-by-the-extracellular-matrix>
- Heim, C., & Nemeroff, C. B. (2001). The role of childhood trauma in the neurobiology of mood and anxiety disorders: Preclinical and clinical studies. *Biological Psychiatry*, 49(12), 1023–1039.
- Horii-Hayashi, N., Sasagawa, T., Matsunaga, W., & Nishi, M. (2015). Development and structural variety of the chondroitin sulfate proteoglycans-contained extracellular matrix in the mouse brain. *Neural Plasticity*, 2015, 1–12.
- Isaacson, J. S., & Scanziani, M. (2011). How inhibition shapes cortical activity. *Neuron*, 72(2), 231–243.
- Janak, P. H., & Tye, K. M. (2015). From circuits to behaviour in the amygdala. *Nature*, 517(7534), 284–292.
- Johnson, S. B., Riis, J. L., & Noble, K. G. (2016). State of the art review: Poverty and the developing brain. *Pediatrics*, 137(4), 1–16.
- Kharazia, V. N., & Weinberg, R. J. (1999). Immunogold localization of AMPA and NMDA receptors in somatic sensory cortex of albino rat. *Journal of Comparative Neurology*, 412(2), 292–302.
- LaBar, K. S., LeDoux, J. E., Spencer, D. D., & Phelps, E. A. (1995). Impaired fear conditioning following unilateral temporal lobectomy in humans. *Journal of Neuroscience*, 15(10), 6846–6855.
- Legaz, I., Olmos, L., Real, M. A., Guirado, S., Davila, J. C., & Medina, L. (2005). Development of neurons and fibers containing calcium binding proteins in the pallial amygdala of mouse, with special emphasis on those of basolateral amygdalar complex. *Journal of Comparative Neurology*, 488, 492–513.
- Malter Cohen, M., Jing, D., Yang, R. R., Tottenham, N., Lee, F. S., & Casey, B. J. (2013). Early-life stress has persistent effects on amygdala function and development in mice and humans. *Proceedings of the National Academy of Sciences of the United States of America*, 110(45), 18274–18278.
- McDonald, A. J., Mascagni, F., Mania, I., & Rainnie, D. G. (2005). Evidence for a perisomatic innervation of parvalbumin-containing interneurons by individual pyramidal cells in the basolateral amygdala. *Brain Research*, 1035(1), 32–40.
- Miyata, S., Komatsu, Y., Yoshimura, Y., Taya, C., & Kitagawa, H. (2012). Persistent cortical plasticity by upregulation of chondroitin 6-sulfation. *Nature Neuroscience*, 15(3), 414–422.
- Moriceau, S., Raineki, C., Holman, J. D., Holman, J. G., & Sullivan, R. M. (2009). Enduring neurobehavioral effects of early life trauma mediated through learning and corticosterone suppression. *Frontiers in Behavioral Neuroscience*, 3, 22.
- Morikawa, S., Ikegaya, Y., Narita, M., & Tamura, H. (2017). Activation of perineuronal net-expressing excitatory neurons during associative memory encoding and retrieval. *Scientific Reports*, 7, 46024.
- Muller, J. F., Mascagni, F., & McDonald, A. J. (2005). Coupled networks of parvalbumin-immunoreactive interneurons in the rat basolateral amygdala. *Journal of Neuroscience*, 25(32), 7366–7376.
- Muller, J. F., Mascagni, F., & McDonald, A. J. (2006). Pyramidal cells of the rat basolateral amygdala: Synaptology and innervation by parvalbumin-immunoreactive interneurons. *Journal of Comparative Neurology*, 494, 635–650.
- Nusser, Z., Lujan, R., Laube, G., Roberts, J. D., Molnar, E., & Somogyi, P. (1998). Cell type and pathway dependence of synaptic AMPA receptor number and variability in the hippocampus. *Neuron*, 21(3), 545–559.
- Pantazopoulos, H., Murray, E. A., & Berretta, S. (2008). Total number, distribution, and phenotype of cells expressing chondroitin sulfate proteoglycans in the normal human amygdala. *Brain Research*, 1207, 84–95.
- Parkes, S. L., & Westbrook, R. F. (2010). The basolateral amygdala is critical for the acquisition and extinction of associations between a neutral stimulus and a learned danger signal but not between two neutral stimuli. *Journal of Neuroscience*, 30(38), 12608–12618.
- Pattwell, S. S., Bath, K. G., Perez-Castro, R., Lee, F. S., Chao, M. V., & Ninan, I. (2012). The BDNF Val66Met polymorphism impairs synaptic transmission and plasticity in the infralimbic medial prefrontal cortex. *Journal of Neuroscience*, 32(7), 2410–2421.
- Paxinos, G., & Watson, C. (1998). *The rat brain in stereotaxic coordinates*. San Diego, CA: Academic Press.
- Perry, R., Finegood, E., Braren, S., DeJoseph, M. L., Putrino, D. F., Wilson, D. A., ... Blair, C. (2018). Developing a neurobehavioral animal model of poverty: Drawing cross-species connections between environments of scarcity-adversity, parenting quality, and infant outcome. *Development and Psychopathology*, 4(2), 1–20.

- Perry, R., & Sullivan, R. M. (2014). Neurobiology of attachment to an abusive caregiver: Short-term benefits and long-term costs. *Developmental Psychobiology*, *56*, 1626–1634.
- Perry, R. E., Al Ain, S., Raineke, C., Sullivan, R. M., & Wilson, D. A. (2016). Development of odor hedonics: Experience-dependent ontogeny of circuits supporting maternal and predator odor responses in rats. *The Journal of Neuroscience*, *36*(25), 6634–6650.
- Pizzorusso, T., Medini, P., Berardi, N., Chierzi, S., Fawcett, J. W., & Maffei, L. (2002). Reactivation of ocular dominance plasticity in the adult visual cortex. *Science*, *298*(5596), 1248–1251.
- Raineke, C., Cortés, M. R., Belnoue, L., & Sullivan, R. M. (2012). Effects of early-life abuse differ across development: Infant social behavior deficits are followed by adolescent depressive-like behaviors mediated by the amygdala. *The Journal of Neuroscience*, *32*(22), 7758–7765.
- Raineke, C., Moriceau, S., & Sullivan, R. M. (2010). Developing a neurobehavioral animal model of infant attachment to an abusive caregiver. *Biological Psychiatry*, *67*(12), 1137–1145.
- Raineke, C., Sarro, E., Rincon-Cortes, M., Perry, R., Boggs, J., Holman, C. J., ... Sullivan, R. M. (2015). Paradoxical neurobehavioral rescue by memories of early-life abuse: The safety signal value of odors learned during abusive attachment. *Neuropsychopharmacology*, *40*(4), 906–914.
- Rainnie, D. G., Mania, I., Mascagni, F., & McDonald, A. J. (2006). Physiological and morphological characterization of parvalbumin-containing interneurons of the rat basolateral amygdala. *The Journal of Comparative Neurology*, *498*(1), 142–161.
- Rincón-Cortés, M., & Sullivan, R. (2016). Emergence of social behavior deficit, blunted corticolimbic activity and adult depression-like behavior in a rodent model of maternal maltreatment. *Translational Psychiatry*, *6*(10), e930.
- Roosendaal, B., McEwen, B. S., & Chattarji, S. (2009). Stress, memory and the amygdala. *Nature Reviews Neuroscience*, *10*(6), 423–433.
- Roth, T. L., & Sullivan, R. M. (2005). Memory of early maltreatment: Neonatal behavioral and neural correlates of maternal maltreatment within the context of classical conditioning. *Biological Psychiatry*, *57*(8), 823–831.
- Ryan, S. J., Ehrlich, D. E., Jasnow, A. M., Daftary, S., Madsen, T. E., & Rainnie, D. G. (2012). Spike-timing precision and neuronal synchrony are enhanced by an interaction between synaptic inhibition and membrane oscillations in the amygdala. *PLoS One*, *7*(4), e35320.
- Sanchez, M., Ladd, C., & Plotsky, P. (2001). Early adverse experience as a developmental risk factor for later psychopathology: Evidence from rodent and primate models. *Development and Psychopathology*, *13*, 419–449.
- Santiago, A., Aoki, C., & Sullivan, R. M. (2017). From attachment to independence: Stress hormone control of ecologically relevant emergence of infants' responses to threat. *Current Opinion in Behavioral Science*, *14*, 78–85.
- Slaker, M., Churchill, L., Todd, R. P., Blacktop, J. M., Zuloaga, D. G., Raber, J., ... Sorg, B. A. (2015). Removal of perineuronal nets in the medial prefrontal cortex impairs the acquisition and reconsolidation of a cocaine-induced conditioned place preference memory. *Journal of Neuroscience*, *35*(10), 4190–4202.
- Smith, Y., Pare, J. F., & Pare, D. (1998). Cat intraamygdaloid inhibitory network: Ultrastructural organization of parvalbumin-immunoreactive elements. *Journal of Comparative Neurology*, *391*(2), 164–179.
- Smith, Y., Pare, J. F., & Pare, D. (2000). Differential innervation of parvalbumin-immunoreactive interneurons of the basolateral amygdaloid complex by cortical and intrinsic inputs. *Journal of Comparative Neurology*, *416*(4), 496–508.
- Stujenske, J. M., Likhtik, E., Topiwala, M. A., & Gordon, J. A. (2014). Fear and safety engage competing patterns of theta-gamma coupling in the basolateral amygdala. *Neuron*, *83*(4), 919–933.
- Suttkus, A., Rohn, S., Weigel, S., Glöckner, P., Arendt, T., & Morawski, M. (2014). AggreCAN, link protein and tenascin-R are essential components of the perineuronal net to protect neurons against iron-induced oxidative stress. *Cell Death & Disease*, *5*(3), e1119.
- Takahashi, L. K., Hubbard, D. T., Lee, I., Dar, Y., & Sipes, S. M. (2007). Predator odor-induced conditioned fear involves the basolateral and medial amygdala. *Behavioral Neuroscience*, *121*(1), 100–110.
- Teicher, M. H., Samson, J. A., Anderson, C. M., & Ohashi, K. (2016). The effects of childhood maltreatment on brain structure, function and connectivity. *Nature Reviews Neuroscience*, *17*(10), 652–666.
- Tottenham, N. (2012). Human amygdala development in the absence of species-expected caregiving. *Developmental Psychobiology*, *54*(6), 598–611.
- Tye, K. M., Prakash, R., Kim, S. Y., Fenno, L. E., Grosenick, L., Zarabi, H., ... Deisseroth, K. (2011). Amygdala circuitry mediating reversible and bidirectional control of anxiety. *Nature*, *471*(7338), 358–362.
- Vazquez-Sanroman, D. B., Monje, R. D., & Bardo, M. T. (2017). Nicotine self-administration remodels perineuronal nets in ventral tegmental area and orbitofrontal cortex in adult male rats. *Addiction Biology*, *22*(6), 1743–1755.
- Wable, G. S., Barbarich-Marsteller, N. C., Chowdhury, T. G., Sabaliauskas, N. A., Farb, C. R., & Aoki, C. (2014). Excitatory synapses on dendritic shafts of the caudal basal amygdala exhibit elevated levels of GABAA receptor alpha4 subunits following the induction of activity-based anorexia. *Synapse*, *68*(1), 1–15.
- Walker, C. D., Bath, K. G., Joels, M., Korosi, A., Larauche, M., Lucassen, P. J., ... Baram, T. Z. (2017). Chronic early life stress induced by limited bedding and nesting (LBN) material in rodents: Critical considerations of methodology, outcomes and translational potential. *Stress*, *20*(5), 421–448.
- Wiedemayer, C. P., & Barr, G. A. (2001). Developmental changes in c-fos expression to an age-specific social stressor in infant rats. *Behavioural Brain Research*, *126*(1–2), 147–157.
- Wolff, S. B., Grundemann, J., Tovote, P., Krabbe, S., Jacobson, G. A., Müller, C., ... Luthi, A. (2014). Amygdala interneuron subtypes control fear learning through disinhibition. *Nature*, *509*(7501), 453–458.
- Woodruff, A. R., & Sah, P. (2007a). Inhibition and synchronization of basal amygdala principal neuron spiking by parvalbumin-positive interneurons. *Journal of Neurophysiology*, *98*(5), 2956–2961.
- Woodruff, A. R., & Sah, P. (2007b). Networks of parvalbumin-positive interneurons in the basolateral amygdala. *Journal of Neuroscience*, *27*(3), 553–563.
- Yang, S., Cacquevel, M., Saksida, L. M., Bussey, T. J., Schneider, B. L., Aebischer, P., ... Spillantini, M. G. (2015). Perineuronal net digestion with chondroitinase restores memory in mice with tau pathology. *Experimental Neurology*, *265*, 48–58.
- Zaitsev, A. V., Gonzalez-Burgos, G., Povysheva, N. V., Kroner, S., Lewis, D. A., & Krimer, L. S. (2005). Localization of calcium-binding proteins in physiologically and morphologically characterized interneurons of monkey dorsolateral prefrontal cortex. *Cerebral Cortex (New York, NY: 1991)*, *15*(8), 1178–1186.

**How to cite this article:** Santiago AN, Lim KY, Opendak M, Sullivan RM, Aoki C. Early life trauma increases threat response of peri-weaning rats, reduction of axo-somatic synapses formed by parvalbumin cells and perineuronal net in the basolateral nucleus of amygdala. *J Comp Neurol*. 2018;526: 2647–2664. <https://doi.org/10.1002/cne.24522>